

AD-A051 240

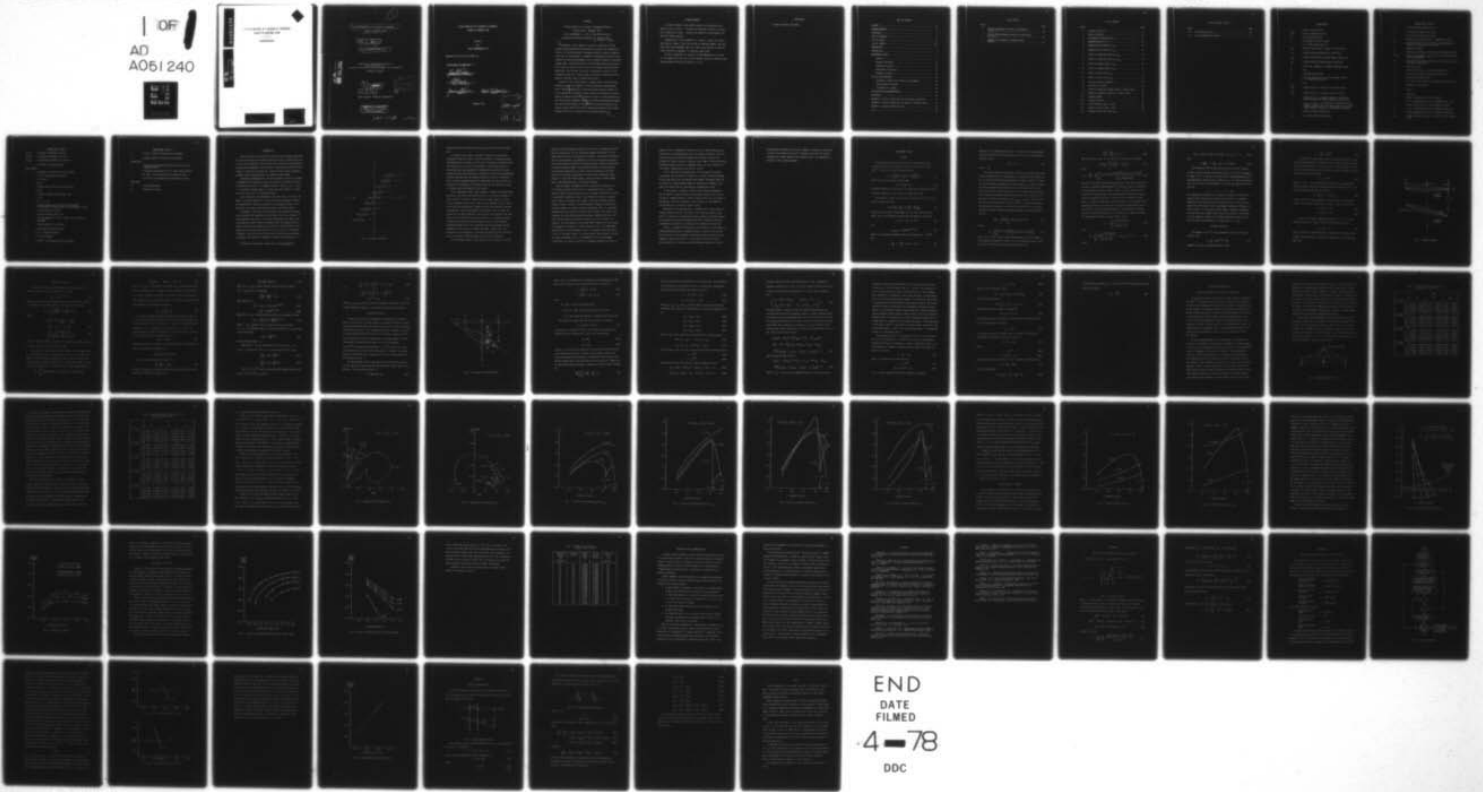
TEXAS A AND M UNIV COLLEGE STATION  
FLUTTER ANALYSIS OF A CASCADE OF STAGGERED BLADES IN SUBSONIC F--ETC(U)  
DEC 77 L KRONENBERGER

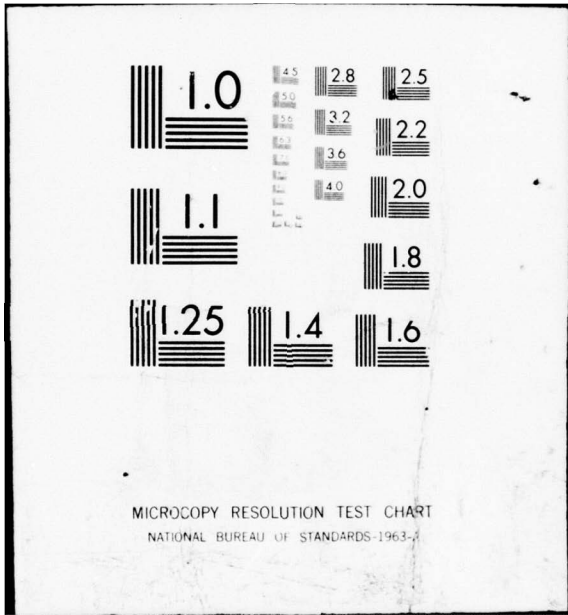
F/G 20/4

UNCLASSIFIED

NL

1 OF  
AD  
A051 240





MICROCOPY RESOLUTION TEST CHART  
NATIONAL BUREAU OF STANDARDS-1963-A

AD A 051240

①

FLUTTER ANALYSIS OF A CASCADE OF STAGGERED  
BLADES IN SUBSONIC FLOW

— \* \* —  
KRONENBERGER

AD No. \_\_\_\_\_  
DDC FILE COPY

DEFENSE RESEARCH AND ENGINEERING AGENCY  
Approved for public release;  
Distribution Unlimited

DDC  
RECORDED  
MAR 16 1978  
R-101105

1

6 FLUTTER ANALYSIS OF A CASCADE OF STAGGERED  
BLADES IN SUBSONIC FLOW.

9 Master's Thesis,

by

10 LOUIS KRONENBERGER, JR.

Submitted to the Graduate College of  
Texas A&M University  
in partial fulfillment of the requirement for the degree of  
MASTER OF SCIENCE

AD NO. \_\_\_\_\_  
DDC FILE COPY

11 Dec 1977

12 76p.

DDC  
RECORDED  
MAR 16 1978  
RECEIVED  
A

Major Subject: Aerospace Engineering

DISTRIBUTION STATEMENT A  
Approved for public release;  
Distribution Unlimited

347 35¢

See

FLUTTER ANALYSIS OF A CASCADE OF STAGGERED  
BLADES IN SUBSONIC FLOW

A Thesis

by

LOUIS KRONENBERGER, JR.

Approved as to style and content by:

\_\_\_\_\_  
(Co-Chairman of Committee)

*Edward A. Carlson*  
\_\_\_\_\_  
(Co-Chairman of Committee)

*A. Cronk*  
\_\_\_\_\_  
(Head of Department)

*James L. Hand*  
\_\_\_\_\_  
(Member)

*Ralph L. Cavitt III*  
\_\_\_\_\_  
(Member)

December 1977

SERIALIZED BY	
YES	NO
YES	NO
MANUSCRIPT	
NOTE	
BY	
RESTRICTING AVAILABILITY CODES	
DATE	AVAIL. CODE OR SPECIAL
A	

## ABSTRACT

Flutter Analysis of a Cascade of Staggered Blades in  
Subsonic Flow. (December 1977)

Louis Kronenberger, Jr., B.S., Texas A&M University

Co-Chairmen of Advisory Committee: Dr. Balusu M. Rao  
Dr. Leland A. Carlson



The purpose of this report is to utilize a numerical lifting surface theory developed by Rao and Jones to predict the unsteady airloads on an infinite cascade of staggered blades in subsonic compressible flow. An investigation is conducted to determine the effect on the unsteady airloads when parameters such as reduced frequency, interblade stagger angle, interblade spacing, and interblade phase lag are varied over a specific range of values. Once the unsteady airloads have been determined, they are used to perform an aeroelastic analysis of the staggered cascade for a single degree of freedom in torsion and a two degree of freedom system in bending and torsion.

Results of the single degree of freedom analysis yields flutter boundaries. These are compared to results obtained by Whitehead who used a different technique for calculating the unsteady airloads on a finite cascade. A new general flutter program is developed for the two degree of freedom system. The airloads are used as forcing functions in the resulting two Lagrangean equations of motion representing the bending and torsional degrees of freedom. The iterative procedure of the flutter program yields the flutter frequency and speed of the cascade reference airfoil as a function of the cascade parameters.



## ACKNOWLEDGEMENTS

The author wishes to give special thanks and recognition to Dr. Balusu M. Rao. In addition to serving as committee chairman, it was Dr. Rao's suggestions, genuine interest, and generous funding support that made this thesis possible.

Recognition is also extended to Dr. Leland A. Carlson, Dr. James L. Rand, and Dr. Ralph K. Cavin for serving as committee members. The time that these three gentlemen took out of their busy schedule in order to offer constructive comments, is sincerely appreciated.

Finally, recognition is certainly due the Department of the Army for the opportunity, the time, and the funding involved in obtaining the advanced degree of which this thesis is a part.

DEDICATION

To Lynda, Michelle, and Kellie.

## TABLE OF CONTENTS

ABSTRACT .....	iii
ACKNOWLEDGEMENTS .....	iv
DEDICATION .....	v
TABLE OF CONTENTS .....	vi
LIST OF TABLES .....	vii
LIST OF FIGURES .....	viii
NOMENCLATURE .....	x
INTRODUCTION .....	1
AERODYNAMIC THEORY .....	7
General .....	7
Boundary Conditions .....	10
Numerical Procedure .....	13
Aerodynamic Derivatives .....	14
Equations of Motion .....	16
RESULTS AND DISCUSSION .....	24
Convergence Studies and Variation of Parameters .....	24
Single Degree of Freedom .....	36
Two Degrees of Freedom .....	42
CONCLUSIONS AND RECOMMENDATIONS .....	47
REFERENCES .....	49
APPENDIX A Physical Interpretation of Resonance Conditions .....	51
APPENDIX B Example Problem for Two Degree of Freedom Flutter ....	53
APPENDIX C Change of Reference Axis .....	59
VITA .....	62

## LIST OF TABLES

Table		Page
1	Effect of Parameter Variation on Aerodynamic Derivatives .....	26
2	Effect of Blade Segment Variation on Aerodynamic Derivatives .....	28
3	Summary of Two Degree of Freedom Flutter Analysis .....	46

## LIST OF FIGURES

Figure		Page
1	Cascade of Airfoils .....	2
2	Blade Coordinates .....	12
3	Two Degree of Freedom Airfoil .....	17
4	Segmented Blade for $N = 4$ .....	25
5	Compressibility Effects on $C_{\ell Z}$ .....	30
6	Compressibility Effects on $C_{m\alpha}$ .....	31
7	Effect of Interblade Spacing on $C_{\ell Z I}$ .....	32
8	Effect of Interblade Spacing on $C_{m\alpha I}$ .....	33
9	Effect of Stagger Angle on $C_{\ell Z I}$ .....	34
10	Effect of Stagger Angle on $C_{m\alpha I}$ .....	35
11	Effect of Phase Lag on $C_{\ell Z I}$ .....	37
12	Effect of Phase Lag on $C_{m\alpha I}$ .....	38
13	Torsional Flutter Boundaries .....	40
14	Sub-Critical Flutter .....	41
15	Effect of Interblade Stagger Angle on Flutter Speed ....	43
16	Effect of Interblade Spacing on Flutter Speed .....	44
A-1	Resonance Model .....	51
B-1	Program Flowchart .....	54
B-2	First Iteration, Mach = 0.500 .....	56
B-3	Second Iteration, Mach = 0.510 .....	56
B-4	Assumed Flutter Mach Prediction .....	58

## LIST OF FIGURES (CONT'D.)

Figure		Page
C-1	Blade Reference Axis .....	59
C-2	Force and Moment Orientation .....	60

## NOMENCLATURE

$a$	= speed of sound, ft/sec.
$a(m)$	= term in exponential series
$A$	= influence coefficient
$B$	= half-width of airfoil segment
$c$	= $2\ell$ = blade chord length, ft.
$C_{\ell z}$	= complex translational unsteady lift coefficient
$C_{\ell \alpha}$	= complex pitching unsteady lift coefficient
$C_{mz}$	= complex translational unsteady moment coefficient
$C_{m \alpha}$	= complex pitching unsteady moment coefficient
$d$	= horizontal component of cascade interblade spacing
$D$	= $d/\ell$
$F$	= generalized force term
$h$	= vertical component of cascade interblade spacing; = $\ell z$ = flapped displacement
$H$	= $\beta h/\ell$
$H_0^{(2)}$	= Hankel function of second kind and zeroth order
$H_1^{(2)}$	= Hankel function of second kind and first order
$I$	= imaginary part of unsteady aerodynamic derivatives; blade mass moment of inertia about the elastic axis
$K$	= $(\phi_{\text{upper}} - \phi_{\text{lower}})$ = discontinuity in modified velocity potential between upper and lower surfaces of an airfoil; complex doublet intensity in transformed coordinates
$K_z$	= bending stiffness coefficient
$K_\alpha$	= torsional stiffness coefficient

## NOMENCLATURE (CONT'D.)

$\ell$	= reference length (semi-chord), ft.
$\tilde{\ell}$	= lift per unit chord per unit span
L	= lift with reference to mid-chord
m	= blades of the cascade; terms in exponential series
M	= local Mach number; nose-up pitching moment about mid-chord axis; blade mass per unit span
N	= segment of airfoil
p	= point on the reference airfoil; blade frequency, rad/sec.
P <sub>1</sub> , P <sub>2</sub>	= roots of the quadratic equation for the real part of the flutter determinant
P <sub>3</sub>	= solution to the linear equation for the imaginary part of the flutter determinant
Q	= velocity, ft/sec.
r	= distance from axis of rotation along blade axis
R	= real part of unsteady aerodynamic derivatives
s	= cascade interblade spacing
S	= $s/\ell = (D^2 + H^2)^{1/2}$ ; blade static moment about elastic axis
S <sub>0</sub>	= exponential series term
S <sub>1</sub>	= $\partial S_0 / \partial X$
t	= time, sec.
T	= kinetic energy per unit span of airfoil
u	= $\partial \phi / \partial x$ = perturbation velocity component along x axis
U	= local velocity, ft/sec.; blade potential energy
w	= $\partial \phi / \partial z$ = perturbation velocity component along z axis
W	= complex downwash velocity in transformed coordinates
W <sub>p</sub>	= complex downwash velocity at a point p on the reference blade

## NOMENCLATURE (CONT'D.)

$(x,z,t)$	= Cartesian coordinates and time
$(X,Z,T)$	= transformed coordinates and time
$(X_p, Z_p)$	= transformed coordinates at a point p
$z$	= amplitude in flapping motion
Greek Symbols	
$\alpha$	= amplitude in pitching or torsional motion
$\beta$	= $(1-M^2)^{\frac{1}{2}}$ = compressibility factor
$\delta$	= $(\sigma + \epsilon D)/2\pi$
$\epsilon$	= $M^2\omega/\beta^2$
$\eta$	= percent blade chord; blade axis position
$\kappa$	= $M\omega/\beta^2$
$\lambda$	= cascade interblade stagger angle, deg.
$\mu$	= $\kappa S/2\pi$
$\nu$	= $(\omega + \epsilon) = \omega/\beta^2$
$\xi$	= cascade stagger angle as defined by Whitehead <sup>9</sup> ; displacement for flapped blade in transformation of axis
$\rho$	= air mass density; slug/ft <sup>3</sup> .
$\sigma$	= cascade interblade phase lag
$\phi$	= velocity potential, ft <sup>2</sup> /sec.; phase lag as defined by Whitehead <sup>9</sup>
$\phi_p$	= velocity potential at a point p
$\Phi$	= transformed velocity potential
$\omega$	= $p\ell/U$ = reduced frequency
$\omega_c$	= critical frequency
$\omega_z$	= $(K_z/M)^{\frac{1}{2}}$ = blade bending natural frequency

## NOMENCLATURE (CONT'D.)

$\omega_\alpha$  =  $(K_\alpha/I)^{1/2}$  = blade torsional natural frequency

$\nabla$  = gradient operator in Cartesian coordinates

## Superscripts

' = indicates non-dimensionalization with respect to the blade semi-chord

- = indicates transformation to axis other than mid-chord

. =  $d(\ )/dt$  = first derivative with respect to time

.. =  $d^2(\ )/dt^2$  = second derivative with respect to time

## Subscripts

le = blade leading edge

te = blade trailing edge

## INTRODUCTION

Many researchers have devoted considerable effort towards predicting the flow characteristics through the multiple stages of blades that exist in axial flow compressors. The research efforts have been concentrated on obtaining the aerodynamic loads utilized in the design of more efficient blades. In addition to the need for information about blade aerodynamic loading, flutter characteristics also need to be determined.

Assuming two-dimensionality, the flow through a single row of blades is mathematically equivalent to the flow through a staggered cascade of infinitely many airfoils. A staggered cascade is shown in Fig. 1, where  $\lambda$  is interblade stagger angle,  $l$  is blade semi-chord length,  $U$  is free-stream velocity, and  $s$  is interblade spacing.

Early researchers like Whitehead<sup>1</sup>, Kemp and Sears<sup>2</sup>, and Schorr and Reddy<sup>3</sup>, assumed incompressible flow and developed aerodynamic theories and computational schemes for predicting the unsteady airloads on the blades for oscillatory freestream flow and/or oscillating blades.

An example is the work of Kemp and Sears<sup>2</sup> who studied the problem of the unsteady lift generated on a reference airfoil of a cascade. In their approach, they used an oscillatory freestream flow. Their study considered the steady interaction between blades but neglected the unsteady interaction and therefore, the effects of cascade spacing. Their approach was to express the unsteady lift as a function of the design parameters, such as the ratio of the airfoil chord and the disturbance wavelength, thus enabling a designer to optimize the performance of a

---

The format of this thesis follows that of the AIAA Journal.

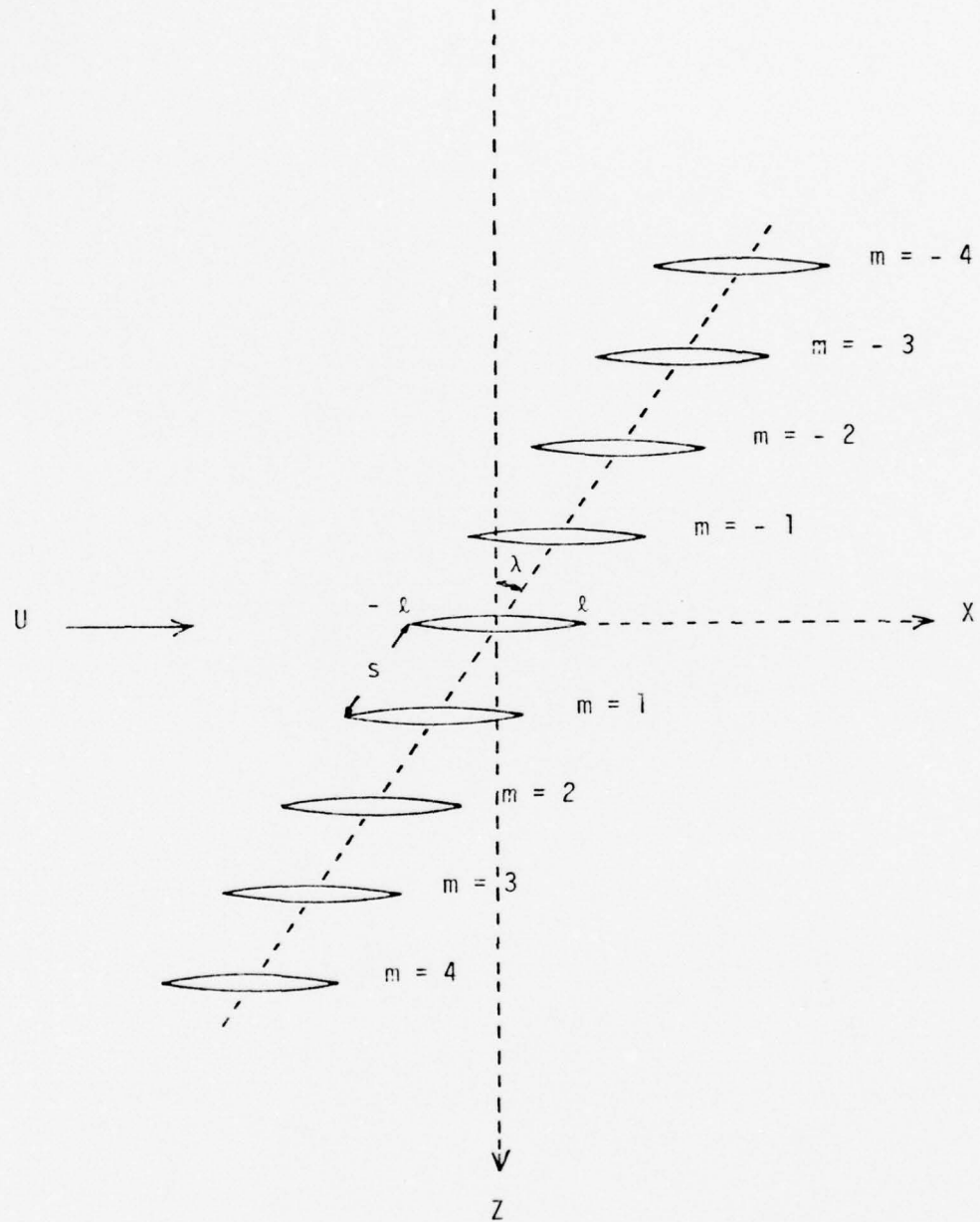


Fig. 1 Cascade of Airfoils.

turbomachine design instead of analyzing one particular blade arrangement.

In another study, Schorr and Reddy<sup>3</sup> treated the flow through a staggered cascade of airfoils in which the effect of unsteady upstream disturbances were included as in the case of unsteady or distorted inlet flow conditions in an axial flow compressor. Their problem was also formulated under the assumption of incompressible potential flow and numerical results were obtained for oscillatory flow using an approximate solution developed from the integral equations involved. In addition, their solution yielded unsteady lift coefficients for the airfoils as a function of the frequency of the oscillations and for different values of stagger angle and solidity of the cascade.

In an independent study, Jones and Moore<sup>4</sup> studied the incompressible flow about a cascade of oscillating airfoils at zero mean incidence. In order to obtain a solution, they utilized a unique numerical lifting surface technique which differs from all other methods in that it makes use of the velocity potential instead of acceleration potential doublet distributions. A major advantage of this method is that it leads to a simpler set of linear equations. Rao and Jones<sup>5</sup> later applied this technique to the oscillatory flow about an airfoil of a staggered cascade. Airload results were obtained for several values of high frequency, interblade stagger angle, and interblade spacing and showed excellent agreement with the results of Schorr and Reddy<sup>3</sup>. Results were also obtained for one combination of interblade stagger angle and interblade spacing at several interblade phase lag angles and frequencies.

In a technique similar to that used by Schorr and Reddy<sup>3</sup>, Fleeter<sup>6</sup>

used oscillating inflow and considered the effects of compressibility on both the fluctuating lift and fluctuating moment coefficients for cascaded airfoils having an upstream non-uniformity. A solution was obtained for the time-dependent, two-dimensional, partial differential equations which describe the perturbation velocity potential through an application of Fourier transform theory. The resulting integral solution equation was evaluated numerically by a matrix inversion technique. The fluctuating lift and moment coefficient variations were computed and represented as a function of Mach number, cascade solidity, cascade stagger angle, interblade phase lag, and reduced frequency.

Jones and Moore<sup>7</sup> extended the velocity potential formulation to oscillating two-dimensional airfoils in compressible flow. In their numerical method they replaced the series of Hankel functions by a rapidly convergent exponential series. They studied the effects of varying airfoil spacing, frequency, Mach number, and phase difference between adjacent blades. Variations in the aerodynamic damping can become zero but never negative at certain discrete frequencies. This is a desirable characteristic with respect to flutter due to bending. The results also indicated that the pitching moment aerodynamic damping relative to the blade quarter-chord axis, while also being zero at the critical frequencies, could be negative at the higher Mach numbers over a wide range of frequencies of interest in flutter analysis. This is an undesirable characteristic from the standpoint that it increases the area of instability for torsional flutter. In a recent paper, Rao and Jones<sup>8</sup> utilized the theory developed in Ref. 7 to determine the airload and moment coefficients on a typical airfoil of a staggered cascade of airfoils in

subsonic flow. Circumferential distortion due to inflow conditions was expressed as an interblade phase lag. The separate conditions for oscillatory inflow and oscillating blades were considered. Results were obtained for several values of frequency, Mach number, interblade spacing, interblade stagger angle, and interblade phase lag. The oscillatory inflow results compared well with those of Fleeter.

In his study utilizing compressible flow, Whitehead<sup>9</sup> presented calculations for the torsional flutter of a cascade of unstalled blades at zero mean deflection and subsonic Mach numbers. Whitehead found that the effect of increasing Mach number was favorable and tended to suppress the flutter that was predicted by incompressible theory.

In this report, a numerical lifting surface theory developed by Rao and Jones<sup>8</sup> is used to predict the unsteady airloads on an infinite cascade of staggered blades in subsonic compressible flow. The effect of the geometric and flow parameters on the airloads is investigated by varying them over a practical range of values.

Additionally, an investigation is conducted for a single degree of freedom system in torsion. The effect of the flow and geometric parameters is evaluated in establishing flutter boundaries and these results are compared with those of Whitehead<sup>9</sup> who used a completely different computational procedure for calculating the aerodynamic derivatives.

Finally, a general flutter program is developed for a two degree of freedom (bending-torsion), staggered cascade in subsonic flow. The geometric portions of the equations of the blade motion are derived using Lagrange's equation of motion<sup>10</sup>. The unsteady airloads are used as forcing functions in the resulting two Lagrangean equations of motion

representing the bending and torsional degrees of freedom. By utilizing an iterative procedure which permits frequency variation, the flutter frequency and flutter speed of the reference airfoil are obtained as a function of the cascade parameters.

## AERODYNAMIC THEORY

## General

The governing equation for the unsteady, compressible, two-dimensional flow of an isentropic, inviscid, irrotational fluid is given<sup>11</sup> in terms of its velocity potential by,

$$\nabla^2 \phi - \frac{1}{a^2} \left[ \frac{\partial^2 \phi}{\partial t^2} + \frac{\partial}{\partial t} (Q^2) + \vec{Q} \cdot \nabla \left( \frac{Q^2}{2} \right) \right] = 0 \quad (1)$$

where  $\phi$  is the perturbation velocity and

$$\vec{Q} = (U+u)\hat{i} + w\hat{k} . \quad (2)$$

Freestream velocity is given as  $U$ . The respective perturbation velocity components along the  $x$  and  $z$  axes are,  $u(=\frac{\partial \phi}{\partial x})$  and  $w(=\frac{\partial \phi}{\partial z})$ .

Assuming that  $u$  and  $w$  are very small compared to  $U$ , Eqs. (1) and (2) are combined to yield,

$$(1-M)^2 \frac{\partial^2 \phi}{\partial x^2} + \frac{\partial^2 \phi}{\partial z^2} = \frac{1}{a^2} \frac{\partial^2 \phi}{\partial t^2} + \frac{2M}{a} \frac{\partial^2 \phi}{\partial x \partial t} , \quad (3)$$

where  $M$  is the freestream Mach number and  $a$  is the speed of sound. Jones<sup>7</sup> used a non-dimensional coordinate transformation such that,

$$X = \frac{x}{\ell} , \quad Z = \beta \frac{z}{\ell} , \quad T = \frac{Ut}{\ell} \quad (4)$$

and

$$\phi(x,z,t) = U\ell\phi(X,Z)e^{i(\epsilon X + \omega T)} \quad (5)$$

where  $\ell$  is a reference length for blade semi-chord and  $\beta = (1-M^2)^{1/2}$ .

Also,

$$\omega = \frac{p\ell}{U} , \quad \epsilon = \frac{M^2\omega}{\beta^2} , \quad \text{and } \phi = \phi(X,Z) . \quad (6)$$

When Eq. (3) is combined with Eq. (5), it reduces to a two-dimensional Helmholtz equation for the perturbation velocity in the transformed coordinate system,

$$\nabla^2 \phi + \kappa^2 \phi = 0 \quad (7)$$

where  $\kappa = \frac{M_{\infty}}{\beta^2}$ .

For a flow problem, the boundary conditions are usually prescribed. For an isolated airfoil in compressible, unsteady flow, the solution of Eq. (7) can be derived by the application of Green's Theorem<sup>12</sup>. A relation for the velocity potential at a given point,  $\phi_p$ , is given in terms of velocity potential distribution over the lifting surface and its wake. Treating the lifting surface as a thin airfoil, the discontinuity in the velocity potential between the upper and lower surfaces is expressed as a doublet distribution,  $K (= \phi_{\text{upper}} - \phi_{\text{lower}})$ . One such solution for an isolated airfoil is given in Ref. 7. The relation between the downwash at any point  $p$  on a thin reference blade on a staggered cascade in subsonic flow and the modified doublet distribution  $K(X)$ , is given as,

$$2\pi W_p = - \int_{-1}^{\infty} K(X) \frac{\partial^2}{\partial Z_p^2} S_0(X_p - X, Z_p, D, H, \sigma) dX \quad (8)$$

where,

$$S_0 = \frac{\pi i}{2} \sum_{m=-\infty}^{\infty} e^{im(\sigma + \epsilon D)} H_0^{(2)} \left\{ \kappa \left[ (X_p - X + mD)^2 + (mH - Z_p)^2 \right]^{1/2} \right\} \quad (9)$$

and  $D = \frac{d}{\ell}$ ,  $H = \frac{\beta h}{\ell}$ , and  $\sigma$  is the interblade phase lag. The blades of the cascade are numbered  $m$ , with  $m = 0$  as the reference airfoil. Since  $S_0$  in Eq. (9) satisfies the wave equation in the form,

$$\frac{\partial^2 S_0}{\partial X^2} + \frac{\partial^2 S_0}{\partial Z^2} + \kappa^2 S_0 = 0 \quad (10)$$

and in the limit as  $Z_p \rightarrow 0$ , Eq. (10) may be rewritten in the form,

$$2\pi W(X_p) = \int_{-1}^{\infty} K(X) \left( \frac{\partial S_1}{\partial X} + \kappa^2 S_0 \right) dX \quad (11)$$

where,

$$S_1 = \frac{\partial S_0}{\partial X} = \frac{\pi i \kappa}{2} \sum_{m=-\infty}^{\infty} e^{im(\sigma + \epsilon D)} \frac{(X_p - X + mD) H_1^{(2)} \left\{ \kappa \left[ (X_p - X + mD)^2 + m^2 H^2 \right]^{1/2} \right\}}{\left[ (X_p - X + mD)^2 + m^2 H^2 \right]^{1/2}} \quad (12)$$

The series involving Hankel functions ( $S_0, S_1$ ) in Eqs. (9) and (12) have very poor convergence characteristics<sup>8</sup>. Therefore, these are replaced by an exponential series as shown in Refs. 13 and 14. However, it is important to understand that this transformation from Hankel function series to exponential series is valid only for an infinite cascade. Hence, it cannot be applied to a finite cascade. The convergence of the exponential series is so good, that the required computational time is less than for a cascade when compared to a two-dimensional isolated airfoil in subsonic flow where it is required to use Hankel functions. The transformed relations as given in Ref. 7 are,

$$S_0 = -\frac{1}{2} \sum_{m=-\infty}^{\infty} \frac{e^{-2\pi a(m) |X_p - X|/S}}{\left[ (\delta - m)^2 - \mu^2 \right]^{1/2}} \quad (13)$$

and,

$$S_1 = \pm \sum_{m=-\infty}^{\infty} \frac{a(m) e^{-2\pi a(m) |X_p - X|/S}}{\left[ (\delta - m)^2 - \mu^2 \right]^{1/2}}, \quad \text{for } X_p > \text{ or } < X, \quad (14)$$

where,

$$a(m) = [(\delta-m)^2 - \mu^2]^{1/2} \frac{H}{S} \pm i(\delta-m) \frac{D}{S}, \quad \text{for } X_p > \text{ or } < X, \quad (15)$$

and,

$$\delta = \frac{\sigma + \epsilon D}{2\pi}, \quad \mu = \frac{\kappa S}{2\pi}, \quad \text{and } S = (D^2 + H^2)^{1/2}. \quad (16)$$

The exponential form of the series  $S_0$  and  $S_1$  not only converge rapidly, but also provides directly the values for critical frequencies as shown in Ref. 7. The Eqs. (13) and (14) will diverge whenever one of the denominators vanishes and no solution of Eq. (11) would be possible. The critical values of the parameter  $\mu$  for which the analysis fails are given by,

$$\mu = \delta, \quad 1 \pm \delta, \quad 2 \pm \delta, \quad \text{etc.}$$

This phenomenon corresponds to a resonance condition at critical frequencies which constitute an infinite set of values of a parameter depending on flow and configuration characteristics at which the aerodynamic function becomes infinite everywhere. Resonance conditions, as shown in App. A, are functions of Mach number, frequency, interblade spacing, phase lag, stagger angle, and acoustic velocity. They represent the condition at which self-induced aerodynamic forces are zero and the blades act effectively as if they were in a vacuum.

#### Boundary Conditions

The downwash  $w (=w'e^{i\omega T})$  can be expressed in terms of  $\phi(X,Z)$  by using Eq. (5),

$$w = \frac{\partial \phi}{\partial Z} = \beta U e^{i(\epsilon X + \omega T)} \frac{\partial \phi}{\partial Z}. \quad (17)$$

Downwash can now be non-dimensionalized to give,

$$W' = \frac{\partial \phi}{\partial Z} = \frac{w' e^{-icX}}{\beta U} \quad (18)$$

Rao and Jones<sup>8</sup> studied the effects of unsteady airloads on a cascade of staggered blades in subsonic flow for both oscillatory inflow and oscillating blades. For the oscillatory inflow condition, Rao and Jones assumed a sinusoidal gust loading such that the downwash boundary conditions on the airfoil were,

$$w'_i = \alpha' e^{i\omega X_i} \quad (19)$$

where  $i = 1, 2, \dots, N$ . For the oscillating blades with flapping and pitching motions about the mid-chord position as shown in Fig. 2, the downwash boundary condition is defined as,

$$w'_i = U \left[ i\omega z' + (1+i\omega X_i)\alpha' \right] \quad (20)$$

where  $z'$  and  $\alpha'$  are the amplitudes in flapping and pitching respectively. Since periodic motions were assumed,  $z$  and  $\alpha$  are defined as,

$$z = z' e^{ipt} = z' e^{i\omega T} \quad (21a)$$

$$\alpha = \alpha' e^{ipt} = \alpha' e^{i\omega T} \quad (21b)$$

The  $K_n$ 's are normally complex and depend on  $z'$  and  $\alpha'$  for any particular values of  $\omega$  and  $M$ . A typical  $K_n$  will have the form,

$$K_n = a_n z' + b_n \alpha' \quad (22)$$

where  $a_n$  and  $b_n$  are complex quantities and depend on frequency, Mach number, interblade spacing, interblade stagger angle, and interblade phase lag.

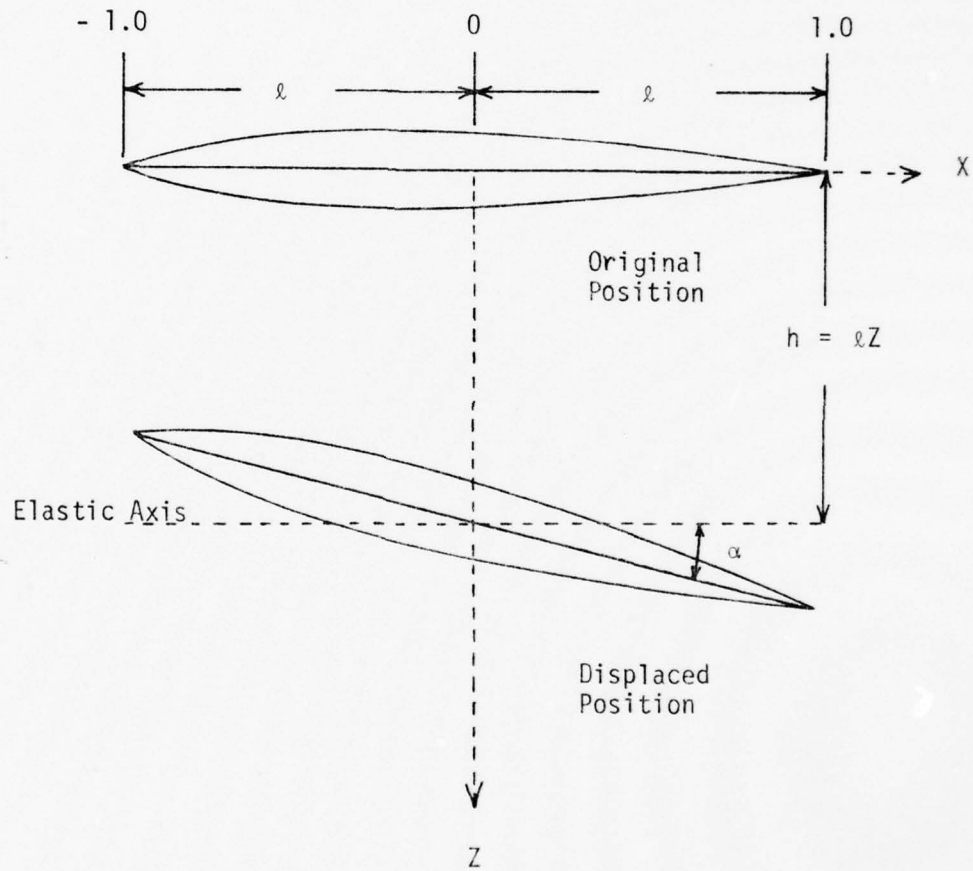


Fig. 2 Blade Coordinates .

## Numerical Procedure

The numerical lifting surface method as developed in Ref. 7 is utilized. The wake boundary condition is given by,

$$K(X) = K_{te} e^{-i\nu(X-1)} \quad (23)$$

where  $K_{te}$  is the doublet strength at the trailing edge ( $X=1$ ). When Eqs. (11) and (23) are combined, they can be expressed in the form,

$$2\pi W_p = \int_{-1}^1 K(X) \left( \frac{\partial S_1}{\partial X} + \kappa^2 S_0 \right) dX + K_{te} I \quad (24)$$

where,

$$I = \int_1^{\infty} e^{-i\nu(X-1)} K_{te} \left( \frac{\partial S_1}{\partial X} + \kappa^2 S_0 \right) dX \\ = -S_{1t} - i\nu S_{0t} - \nu^2 (1-M^2) P \quad (25)$$

$$P = -\frac{1}{2} \sum_{m=-\infty}^{\infty} \frac{S e^{-2\pi a(m)(1-X_p)/S}}{[2\pi a(m) + i\nu S] [(\delta-M)^2 - \mu^2]^{\frac{1}{2}}} \quad (26)$$

and  $a(m) = [(\delta-m)^2 - \mu^2]^{\frac{1}{2}} \frac{H}{S} - i(\delta-m) \frac{D}{S}$ . The symbols  $S_{0t}$  and  $S_{1t}$  represent  $S_0$  and  $S_1$  respectively at the trailing edge.

The airfoil is divided into  $N$  equal strips and  $K$  is assumed to be  $K_n$ , a constant over the  $n$ th strip, where  $n = 1, 2, \dots, N$ . Let  $2B$  be the width of each strip and  $X_n$  denote the center of the  $n$ th strip. In Eq. (24),  $X_p$  and  $W_p$  are replaced by  $X_i$  and  $W_i$  respectively, where  $i$  refers to the  $i$ th strip. Hence, Eq. (24) will then be given approximately by,

$$2\pi W_i = \sum_{n=1}^N K_n \left[ S_1(X_i - X_n - B) - S_1(X_i - X_n + B) + 2\kappa^2 B S_0(X_i - X_n) \right]$$

$$+ K_{te} I(X_i), \quad \text{where } i = 1, 2, \dots, N. \quad (27)$$

When  $X_i = X_n$ ,  $S_0$  is evaluated by integrating the exponential form of  $S_0$  over the interval  $X_n - B < X < X_n + B$ . For other intervals,  $X_i \neq X_n$  and  $S_0$  can either be found by integration or be taken as the mean value of  $S_0$  over the interval.  $K_{te}$  can be expressed as a function of  $K_n$  by using the wake condition. This relation is given by,

$$K_{te} = \frac{K_n}{(2i\nu B + e^{-i\nu B})}. \quad (28)$$

For a given geometry and flow conditions, the numerical terms in Eq. (27) can be evaluated by using Eqs. (13), (14), (25), and (26). For a known set of  $W_j$ 's, Eq. (27) reduces to a system of  $N$  equations with  $N$  unknowns,  $K_1, K_2, \dots, K_N$ , when it is combined with Eq. (28). It is assumed that  $W_j$  is known over the airfoil. In Eq. (27), this represents a set of linear algebraic equations given by,

$$2\pi\{W_j\} = [A]\{K\}. \quad (29)$$

Therefore, knowing the values of  $\{W_j\}$  and  $[A]$  allows for the determination of the doublet distribution,  $\{K\}$ .

#### Aerodynamic Derivatives

Euler's equation of motion is given<sup>15</sup> as,

$$\frac{\partial u}{\partial t} + U \frac{\partial u}{\partial x} = - \frac{1}{\rho} \frac{\partial p}{\partial x}. \quad (30)$$

In terms of the upper and lower velocity potential and pressure on the airfoil, Eq. (30) can be shown to be,

$$\frac{\partial k}{\partial t} + U \frac{\partial k}{\partial x} = \frac{1}{\rho} (p_l - p_u) \quad (31)$$

where  $k(x) = (\phi_u - \phi_l)$ . Since lift per unit chord per unit span is

$\tilde{l}(x) = (p_l - p_u)$ , Eq. (31) becomes,

$$\rho \left( \frac{\partial k}{\partial t} + U \frac{\partial k}{\partial x} \right) = \tilde{l}(x) . \quad (32)$$

Now from Eq. (5),

$$k(x) = \phi_u - \phi_l = U \ell (\phi_u - \phi_l) e^{i(\epsilon X + \omega T)} \quad (33a)$$

$$k(x) = U \ell K(X) e^{i(\epsilon X + \omega T)} , \quad (33b)$$

where  $K(X) = (\phi_u - \phi_l)$ . Equations (32) and (33) are combined to yield,

$$\tilde{l}(X) = \rho U^2 \left[ i\nu K(X) + \frac{\partial K(X)}{\partial X} \right] e^{i(\epsilon X + \omega T)} \quad (34)$$

where  $\nu = \omega/\beta^2$ . Equation (34) is valid on the airfoil surface,

$-1 \leq X \leq 1$ . In the wake region, no pressure discontinuities are allowed to exist and hence,

$$i\nu K(X) + \frac{\partial K(X)}{\partial X} = 0 \quad (35)$$

must be satisfied when  $X \geq 1$ .

When values of  $K_n$  have been obtained, the local lift,  $\tilde{l}$ , at a point  $X$  is given by Eq. (34). If  $\bar{K}$  is substituted for  $K e^{i\epsilon X}$ , then

$$\frac{\tilde{l}(X)}{\rho U^2 \ell} = (i\omega \bar{K} + \frac{\partial \bar{K}}{\partial X}) e^{i\omega T} \quad (36a)$$

$$\frac{\tilde{l}(X)}{\rho U^2 \ell} = (i\omega \bar{K} + \frac{\partial \bar{K}}{\partial X}) e^{ipt} \quad (36b)$$

The lift  $L(=L' e^{ipt})$  and the nose-up pitching moment about the mid-chord axis  $M(=M' e^{ipt})$  are given by,

and,

$$\frac{L'}{\rho U^2 \ell} = \bar{K}_{te} + i\omega \int_{-1}^1 \bar{K} dX = C_{\ell z} z' + C_{\ell \alpha} \alpha' \quad (37)$$

$$\begin{aligned} \frac{M'}{\rho U^2 \ell^2} &= \bar{K}_{te} + \int_{-1}^1 \bar{K} dX - i\omega \int_{-1}^1 X \bar{K} dX \\ &= C_{mz} z' + C_{m\alpha} \alpha' \end{aligned} \quad (38)$$

where  $C_{\ell z}$ ,  $C_{\ell \alpha}$ ,  $C_{mz}$ , and  $C_{m\alpha}$  are the aerodynamic derivatives. These are usually complex and depend on the geometry and flow characteristics.

#### Equations of Motion

Flutter can be defined as the dynamic instability of an elastic body in an airstream. A dynamic system is assumed to flutter at a speed where the net damping forces are equal to zero. There exists a frequency at which flutter occurs. This is termed the flutter frequency. Consider the spring supported airfoil given in Fig. 3 where  $K_z$  and  $K_\alpha$  are stiffness in bending and torsion, respectively. The blade segment is permitted freedom to execute small periodic vertical displacements,  $z(=z' e^{ipt})$ , and angular displacements,  $\alpha(=\alpha' e^{ipt})$ , where  $U$  is free-stream velocity and an oscillation frequency of  $p$  rad/sec. The cascade parameters associated with a staggered row of thin oscillating blades are presented in Fig. 1.

For the reference airfoil, the expression for the kinetic energy per unit span for a mass element  $dm$  undergoing this motion, that is at a distance  $r$  from the rotation point is,

$$dT = \frac{1}{2}(\ell \dot{z} + r \dot{\alpha})^2 dm \quad (39)$$

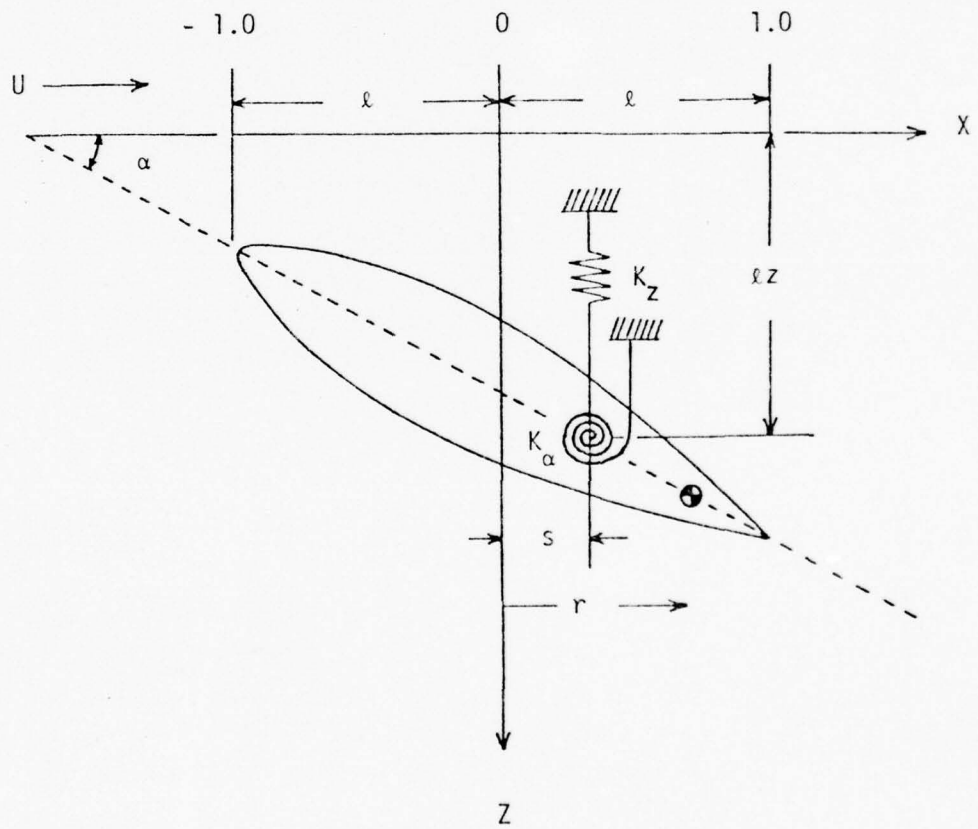


Fig. 3 Two Degree of Freedom Airfoil.

where  $z$  and  $\alpha$  are nondimensional coordinates. By integrating Eq. (39), the kinetic energy per unit span of the airfoil is given by,

$$T = \frac{1}{2} \int_{-l}^l (\ell \dot{z} + r \dot{\alpha})^2 dm \quad (40)$$

$$T = \frac{1}{2} M \ell^2 \dot{z}^2 + S \ell \dot{z} \dot{\alpha} + \frac{1}{2} I \dot{\alpha}^2 \quad (41)$$

where,

$$M = \int dm = \text{blade mass per unit span.}$$

$$S = \int r dm = \text{blade static moment about elastic axis.}$$

$$I = \int r^2 dm = \text{blade mass moment of inertia about elastic axis.}$$

The potential energy expression for the blade is given by,

$$U = \frac{1}{2} K_z \ell^2 z^2 + \frac{1}{2} K_\alpha \alpha^2 \quad (42)$$

The bending and torsional stiffness coefficients are related to the respective natural frequencies,  $\omega_z$  and  $\omega_\alpha$ , by the relations,

$$K_z = M \omega_z^2 \quad (43a)$$

$$K_\alpha = I \omega_\alpha^2 \quad (43b)$$

Flutter is a self-exciting aeroelastic phenomenon involving the interaction between the inertial, elastic, and aerodynamic forces. The structural damping of the blade can be neglected compared to the aerodynamic damping terms associated with the forcing function. Neglecting the structural damping, Lagrange's equations of motion can be expressed as,

$$\frac{d}{dt} \left( \frac{\partial T}{\partial \dot{q}_k} \right) - \frac{\partial T}{\partial q_k} + \frac{\partial U}{\partial q_k} = F_k \quad (44)$$

where  $F_k$  and  $q_k$  are generalized forces and coordinates. The aerodynamic forcing functions are obtained from the two-dimensional unsteady airloads prediction method and are given in the form,

$$F_z = -\rho U^2 (C_{\ell z} z + C_{\ell \alpha} \alpha) \quad (45a)$$

$$F_\alpha = \rho U^2 \ell^2 (C_{mz} z + C_{m\alpha} \alpha) \quad (45b)$$

where  $C_{\ell z}$ ,  $C_{\ell \alpha}$ ,  $C_{mz}$ , and  $C_{m\alpha}$  are the complex aerodynamic derivatives referred to the elastic axis and are given in real and imaginary terms as,

$$C_{\ell z} = C_{\ell zR} + iC_{\ell zI} \quad (46a)$$

$$C_{\ell \alpha} = C_{\ell \alpha R} + iC_{\ell \alpha I} \quad (46b)$$

$$C_{mz} = C_{mzR} + iC_{mzI} \quad (46c)$$

$$C_{m\alpha} = C_{m\alpha R} + iC_{m\alpha I} \quad (46d)$$

Now Eqs. (41), (42), and (45) are combined with Eq. (44) to obtain,

$$M\ddot{z} + S\ddot{\alpha} + K_z \ell z = -\rho U^2 \ell (C_{\ell z} z + C_{\ell \alpha} \alpha) \quad (47a)$$

$$S\ell \ddot{z} + I\ddot{\alpha} + K_\alpha \alpha = \rho U^2 \ell^2 (C_{mz} z + C_{m\alpha} \alpha) \quad (47b)$$

The solutions of Eqs. (47) are assumed to have periodic motion given by,

$$z = z' e^{ipt} \quad (48a)$$

$$\alpha = \alpha' e^{ipt} \quad (48b)$$

Substitution of Eqs. (48) into Eqs. (47) and combining terms,

$$(\ell K_z - M\ell p^2 + \rho U^2 \ell C_{\ell z}) z' + (\rho U^2 \ell C_{\ell \alpha} - S p^2) \alpha' = 0 \quad (49a)$$

$$-(\rho U^2 \ell^2 C_{mz} + S\ell p^2) z' + (K_\alpha - \rho U^2 \ell^2 C_{m\alpha} - I p^2) \alpha' = 0 \quad (49b)$$

Equations (49) are a set of two simultaneous, linear, homogeneous, algebraic equations in  $z'$  and  $\alpha'$ . For this system to have a non-trivial solution, the coefficient determinant of  $z'$  and  $\alpha'$  must be equal to zero.

$$\begin{vmatrix} (\ell K_Z - M\ell p^2 + \rho U^2 \ell C_{\ell Z}) & (\rho U^2 \ell C_{\ell \alpha} - Sp) \\ -(C_{mZ} \rho U^2 \ell^2 + S\ell p^2) & (K_\alpha - \rho U^2 \ell^2 C_{m\alpha} - Ip^2) \end{vmatrix} = 0 \quad (50)$$

This determinant is referred to as the flutter determinant and the solution gives the flutter frequency. However, a direct solution cannot be obtained since the aerodynamic derivatives are functions of  $\omega (=p\ell/U)$ . The aerodynamic derivatives are complex quantities and thus the flutter determinant can be expressed in two parts, real and imaginary. After expanding the flutter determinant and substituting appropriate values of Eqs. (46), the real part becomes,

$$\begin{aligned} & [\ell K_Z K_\alpha] \bar{P}^2 - [\ell K_Z (I + \frac{\rho \ell^4}{\omega^2} C_{m\alpha R}) + K_\alpha (M\ell - \frac{\rho \ell^3}{\omega^2} C_{\ell Z R})] \bar{P} + \\ & [(M\ell I - S^2 \ell) - \frac{\rho \ell^3}{\omega^2} (IC_{\ell Z R} - M\ell^2 C_{m\alpha R} + S\ell C_{mZ R} - S\ell C_{\ell \alpha R}) \\ & - \frac{\rho^2 \ell^7}{\omega^4} (C_{\ell Z R} C_{m\alpha R} - C_{\ell Z I} C_{m\alpha I} + C_{\ell \alpha I} C_{mZ I} - C_{\ell \alpha R} C_{mZ R})] = 0 \end{aligned} \quad (51)$$

and the imaginary part becomes,

$$\begin{aligned} & [K_\alpha C_{\ell Z I} - \ell^2 K_Z C_{m\alpha I}] \bar{P} + [S\ell C_{\ell \alpha I} - IC_{\ell Z I} + M\ell^2 C_{m\alpha I} - S\ell C_{mZ I} \\ & + \frac{\rho \ell^4}{\omega^2} (C_{\ell \alpha R} C_{mZ I} + C_{\ell \alpha I} C_{mZ R} - C_{\ell Z R} C_{m\alpha I} - C_{\ell Z I} C_{m\alpha R})] = 0 \end{aligned} \quad (52)$$

where  $\bar{P} = \frac{1}{p^2}$ . If the real and imaginary parts are set equal to zero,

solutions P1 and P2 can be obtained for the real part and P3 for the imaginary part. For an assumed value of  $\omega$ , if one of the solutions, P1 or P2, of the real part is equal to the solution P3 of the imaginary part, then this  $\omega$  corresponds to the flutter frequency. The main objective is to find the flutter speed. However, the aerodynamic derivatives are functions of the Mach number and the reduced frequency. The flutter problem can only be solved after the aerodynamic derivatives are evaluated. It is necessary to assume a Mach number and a reduced frequency and test whether flutter occurs at these values. If the test results are negative, then it is necessary to iterate on reduced frequency until a flutter speed is obtained for the assumed Mach number. If the two speeds are not equal, then it is necessary to iterate on Mach number until the flutter Mach number is equal to the assumed Mach number. A computational example is illustrated in App. B.

The reference airfoil as illustrated in Fig. 3, with its center at the origin of coordinates, is assumed to be describing plunging and pitching oscillations of frequency  $p$  rad/sec., defined by  $z$  and  $\alpha$ . For a single degree of freedom of flapping reference blade, the equation of motion is given by,

$$M\ddot{z} + K_z z = L_z z \quad (53)$$

where  $z$  is defined for periodic motion as,

$$z = z' e^{ipt} \quad (54)$$

$$\frac{\partial z}{\partial t} = z' i p e^{ipt} = ipz \quad (55)$$

$L_z$  is a complex quantity with real and imaginary components.

$$L_z = L_{zR} + iL_{zI} \quad (56)$$

Now Eqs. (55) and (56) will give,

$$L_z z = zL_{zR} + izL_{zI} = zL_{zR} + \frac{\dot{z}}{p} L_{zI} \quad (57)$$

and Eq. (53) now becomes,

$$M\ddot{z} - \frac{\dot{z}}{p} L_{zI} + (K_z - L_{zR})z = 0. \quad (58)$$

when like terms of Eq. (58) are compared to,

$$M\ddot{z} + C_L \dot{z} + Kz = 0. \quad (59)$$

The damping constant,  $C_L$ , becomes a function of the imaginary part of the lift coefficient in flapping.

$$C_L = - \frac{L_{zI}}{p} \quad (60)$$

In a similar manner, if a single degree of freedom in pitching is considered, the equation of motion is given by,

$$I\ddot{\alpha} + K_\alpha \alpha = M_\alpha \alpha \quad (61)$$

where,

$$\alpha = \alpha' e^{ipt} \quad (62a)$$

$$\dot{\alpha} = \alpha' ipe^{ipt} = ip\alpha \quad (62b)$$

and considering the fact that  $M_\alpha$  is also a complex quantity given as,

$$M_\alpha = M_{\alpha R} + iM_{\alpha I}. \quad (63)$$

It can be shown that,

$$I\ddot{\alpha} - \frac{\dot{\alpha}}{p} M_{\alpha I} + \alpha(K_\alpha - M_{\alpha R}) = 0 \quad (64)$$

and the damping constant,  $C_M$ , is a function of the imaginary part of the moment in pitching.

$$C_M = - \frac{M_{\alpha I}}{p} \quad (65)$$

## RESULTS AND DISCUSSION

## Convergence Studies and Variation of Parameters

A convergence study was conducted utilizing a program developed by B.M. Rao<sup>16</sup>. This program used the numerical lifting surface technique to derive the aerodynamic derivatives for a cascade of staggered blades. In the analysis, the downwash induced at the reference airfoil by the doublet distribution,  $K(X)$ , over each oscillating blade of the cascade is represented by a series of Hankel functions denoted by  $S_0$ . This series, in the form presented, is poorly convergent. However, it has been shown in Refs. 13 and 14 that it can be replaced by a rapidly convergent series of exponential terms. The problem was evaluated using the alternative exponential form of  $S_0$  and its derivative form of  $S_1 (= \partial S_0 / \partial X)$ .

An influencing parameter in the convergence of the exponential function is the number of terms that are included in the series before it converges to an acceptable value. While the value of the exponential series is dependent on the sum of the number of terms considered, a change of  $1 \times 10^{-5}$  was established as a constraint criterion between two consecutive terms for convergence or until a prescribed limit on the number of terms included in the series was reached. In the program,  $NNN (= 2L + 1)$ , where  $L$  is any integer from 1 to  $\infty$ ) was the control parameter that was varied in order to determine the maximum limit of terms that could be summed in the series. Naturally, the greater number of terms would tend to converge on a more accurate value for the series.

However, in the interest of program efficiency, a compromise value for NNN had to be determined and accepted. Table 1 shows typical results obtained for various values of NNN while varying  $\omega$  from 0.10 to 0.40, dividing the reference blade into 16 segments, with an interblade stagger angle of 45 degrees, Mach number of 0.60, interblade phase lag of 90 degrees, and a blade to semi-chord space ratio of 2.0. As is shown in the table, the influence of NNN on the aerodynamic derivatives when it is greater than 100 becomes insignificant. Therefore, a value of NNN equal to 100 was chosen for computational purposes.

An additional program parameter that was considered in the convergence study was that of the number of segments on a typical airfoil. Consider the two-dimensional airfoil as shown in Fig. 4. The blade is divided into  $N$  segments with the coordinate axis located at the mid-chord of the blade and a collocation point,  $X_i$ , located at the center of each segment (where  $i = 1, 2, \dots, N$ ). The doublet distribution,  $K(X)$ , over each segment is assumed to be constant.

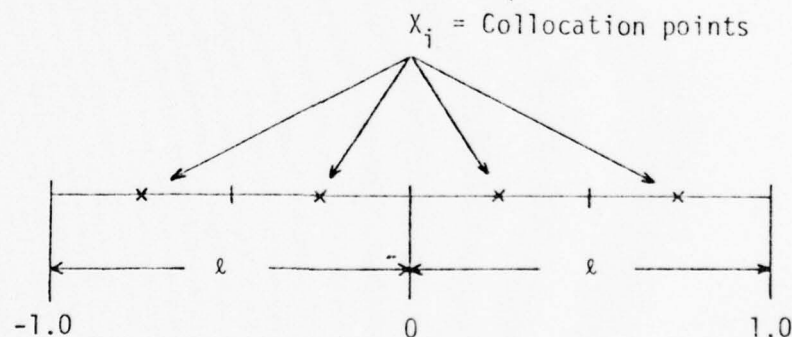


Fig. 4 Segmented Blade for  $N = 4$ .

Table 1 Effect of Parameter Variation on Aerodynamic Derivatives

	NNN		
	50	100	150
$\omega = 0.10$			
$C_{\ell Z}$	0.2895 + 0.6259i	0.2895 + 0.6260i	0.2895 + 0.6260i
$C_{\ell \alpha}$	6.4762 - 2.6460i	6.4766 - 2.6467i	6.4766 - 2.6467i
$C_{mZ}$	0.2356 + 0.2811i	0.2357 + 0.2811i	0.2357 + 0.2811i
$C_{m\alpha}$	2.9262 - 2.4431i	2.9263 - 2.4439i	2.9263 - 2.4439i
$\omega = 0.20$			
$C_{\ell Z}$	0.5423 + 1.0312i	0.5425 + 1.0312i	0.5425 + 1.0312i
$C_{\ell \alpha}$	5.5959 - 2.3289i	5.5963 - 2.3298i	5.5964 - 2.3299i
$C_{mZ}$	0.4771 + 0.4295i	0.4773 + 0.4295i	0.4773 + 0.4295i
$C_{m\alpha}$	2.3739 - 2.6314i	2.3739 - 2.6322i	2.3739 - 2.6323i
$\omega = 0.30$			
$C_{\ell Z}$	0.6376 + 1.3361i	0.6378 + 1.3362i	0.6379 + 1.3362i
$C_{\ell \alpha}$	5.0769 - 1.6554i	5.0774 - 1.6563i	5.0774 - 1.6565i
$C_{mZ}$	0.6689 + 0.5233i	0.6691 + 0.5233i	0.6691 + 0.5233i
$C_{m\alpha}$	2.0558 - 2.6647i	2.0558 - 2.6656i	2.0558 - 2.6657i
$\omega = 0.40$			
$C_{\ell Z}$	0.5794 + 1.6506i	0.5798 + 1.6508i	0.5799 + 1.6508i
$C_{\ell \alpha}$	4.9109 - 0.8886i	4.9117 - 0.8896i	4.9118 - 0.8900i
$C_{mZ}$	0.8300 + 0.6197i	0.8303 + 0.6197i	0.8304 + 0.6197i
$C_{m\alpha}$	1.9325 - 2.7085i	1.9325 - 2.7096i	1.9325 - 2.7098i

The number of segments chosen directly influences the value of the integral evaluated to determine the downwash at each collocation point. Since a larger number of segments will converge to an increasingly more accurate value, a study was conducted to determine the most significant number of segments along the blade to be used. While a minimum of four segments could be used, the degree of confidence in the downwash values increases for segments greater than  $N = 10$ . The program evaluates the downwash integral using a Simpson's three-eighths rule scheme. Additionally, the first and last half-segment are evaluated by using the trapezoidal rule. This requires multiples of  $N(=3L+1)$ , where  $L$  is an integer) segments to be used. Table 2 shows the typical influence that varying  $N$  has on the aerodynamic derivatives. While  $N = 16$  provides reasonable accuracy,  $N = 22$  was chosen to be used throughout the program computations. Theoretically, the greater the number of segments chosen, the greater the accuracy of the aerodynamic derivatives. However, because of the way the solution technique is employed, it is possible that numerical instabilities could be present for values when  $N$  becomes much greater than twenty-five.

For flutter studies, the aerodynamic derivatives  $C_{\ell Z}$  and  $C_{m\alpha}$  provide meaningful information and are shown for several sets of the geometric and flow parameters. Figures 5 thru 12 show the out-of-phase components,  $(C_{\ell Z I}$  and  $C_{m\alpha I})$ , of  $C_{\ell Z}$  and  $C_{m\alpha}$  which represents the damping terms in pure translational and pitching motions, respectively. The sign convention used is such that the negative values of  $C_{m\alpha}$  represent the positive damping constant and the positive values of

Table 2 Effect of Blade Segment Variation on Aerodynamic Derivatives

	N		
	10	16	22
$\omega = 0.10$			
$C_{\ell Z}$	0.4527 + 0.7491i	0.4520 + 0.7456i	0.4518 + 0.7436i
$C_{\ell \alpha}$	7.8324 - 4.2956i	7.8069 - 4.2766i	7.7898 - 4.2694i
$C_{mZ}$	0.3850 + 0.2888i	0.3796 + 0.2785i	0.3764 + 0.2736i
$C_{m\alpha}$	3.0517 - 4.0351i	2.9508 - 3.9835i	2.9015 - 3.9533i
$\omega = 0.20$			
$C_{\ell Z}$	0.8705 + 1.1571i	0.8637 + 1.1504i	0.8604 + 1.1460i
$C_{\ell \alpha}$	6.4617 - 4.0992i	6.4427 - 4.0465i	6.4265 - 4.0220i
$C_{mZ}$	0.7579 + 0.3255i	0.7453 + 0.3115i	0.7381 + 0.3053i
$C_{m\alpha}$	1.8926 - 4.3011i	1.8251 - 4.2449i	1.7945 - 4.2109i
$\omega = 0.30$			
$C_{\ell Z}$	1.1271 + 1.4766i	1.1133 + 1.4715i	1.1062 + 1.4672i
$C_{\ell \alpha}$	5.8947 - 3.5670i	5.8968 - 3.4960i	5.8898 - 3.4613i
$C_{mZ}$	1.0689 + 0.2647i	1.0540 + 0.2505i	1.0454 + 0.2451i
$C_{m\alpha}$	1.1571 - 4.4691i	1.1128 - 4.4309i	1.0961 - 4.4050i
$\omega = 0.40$			
$C_{\ell Z}$	1.3239 + 1.8643i	1.3050 + 1.8638i	1.2948 + 1.8613i
$C_{\ell \alpha}$	5.9616 - 3.2626i	5.9857 - 3.1835i	5.9889 - 3.1432i
$C_{mZ}$	1.3968 + 0.1313i	1.3843 + 0.1145i	1.3768 + 0.1094i
$C_{m\alpha}$	0.5074 - 4.8649i	0.4686 - 4.8520i	0.4579 - 4.8383i
$\omega = 0.50$			
$C_{\ell Z}$	1.6653 + 2.3449i	1.6441 + 2.3510i	1.6321 + 2.3522i
$C_{\ell \alpha}$	6.3849 - 3.6512i	6.4326 - 3.5719i	6.4488 - 3.5294i
$C_{mZ}$	1.7879 - 0.2137i	1.7789 - 0.2393i	1.7742 - 0.2463i
$C_{m\alpha}$	-0.5799 - 5.5162i	-0.6328 - 5.5249i	-0.6457 - 5.5244i

$C_{\ell z I}$  represent positive translational stability.

Figures 5 and 6 show the compressibility effects ( $M = 0.3, 0.5, 0.7,$  and  $0.8$ ) on  $C_{\ell z}$  and  $C_{m\alpha}$  when  $s = 2\ell$ ,  $\lambda = 45^\circ$ , and  $\sigma = 180^\circ$  as  $\omega$  is varied from 0.1 to 0.5. The absolute values of  $C_{\ell z}$  are shown to increase as  $\omega$  increases for Mach numbers less than  $M = 0.7$  and undergoes rapid changes for  $M = 0.8$ . For the parameters considered at  $M = 0.8$  in Fig. 5, there is a rapid change for values between  $\omega = 0.40$  and  $\omega = 0.51$ . The lowest critical frequency occurs at  $\omega = 0.51$ . Figure 6 shows a tendency toward larger changes at the higher  $M = 0.8$  value. As the Mach number increases, the maximum value of damping also increases. This indicates a stabilizing influence in damping as Mach number increases.

Figures 7 and 8 show the effect of interblade spacing ( $s = 1.6\ell$ ,  $2.0\ell$ , and  $2.4\ell$ ) on  $C_{\ell z I}$  and  $C_{m\alpha I}$ , respectively when  $M = 0.8$ ,  $\lambda = 45^\circ$ , and  $\sigma = 180^\circ$  as  $\omega$  is varied from 0.1 to 0.5. For the parameters and the range of frequencies considered, the critical frequencies are for  $s = 1.6\ell$ ,  $\omega_c = 0.64$ ;  $s = 2.0\ell$ ,  $\omega_c = 0.51$ ; and for  $s = 2.4\ell$ ,  $\omega_c = 0.42$ . Both figures indicate that as the interblade spacing increases, the lowest critical frequency decreases. As  $\omega$  increases, the damping decreases rapidly to zero at  $\omega = \omega_c$  and then increases again as  $\omega$  is increased without becoming negative. Below the first critical frequency, the damping decreases when the spacing between the blades is increased.

Figures 9 and 10 show the effect of blade stagger angle ( $\lambda = 0^\circ$ ,  $45^\circ$ , and  $60^\circ$ ) on  $C_{\ell z I}$  and  $C_{m\alpha I}$ , respectively when  $M = 0.8$ ,  $s = 2.0\ell$ , and  $\sigma = 180^\circ$ , as  $\omega$  is varied from 0.1 to 0.5. For the parameters and the range of frequency values considered, the critical frequency values

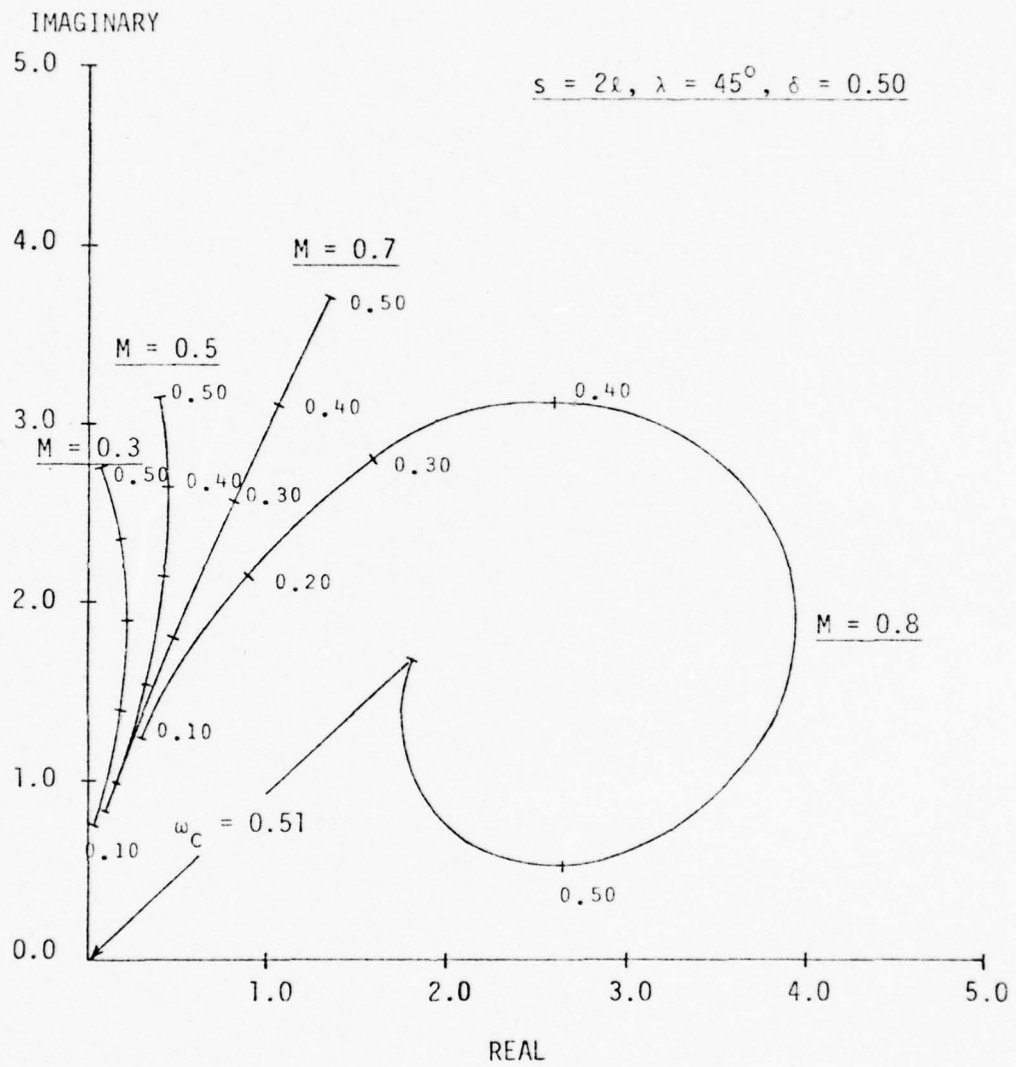


Fig. 5 Compressibility Effects on  $C_{kz}$ .

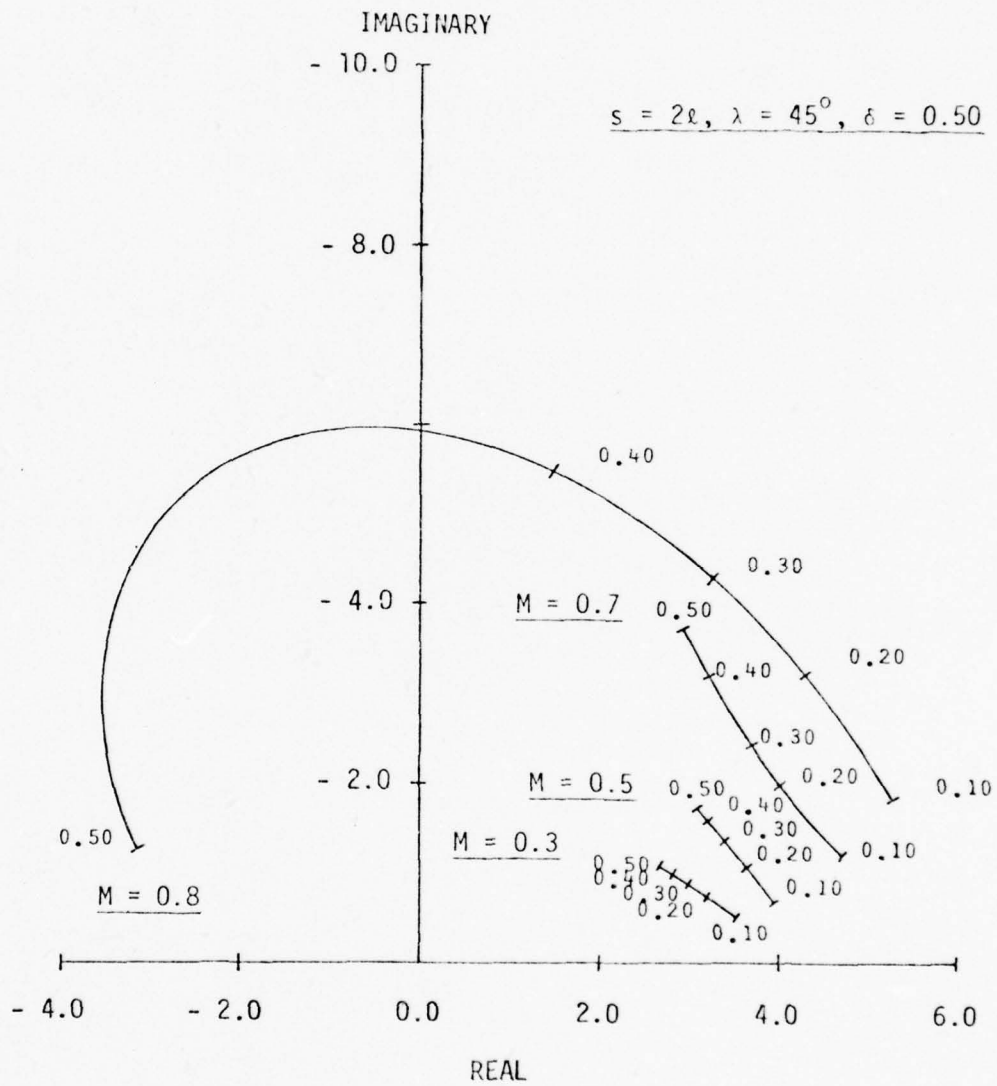


Fig. 6 Compressibility Effects on  $C_{m\alpha}$ .

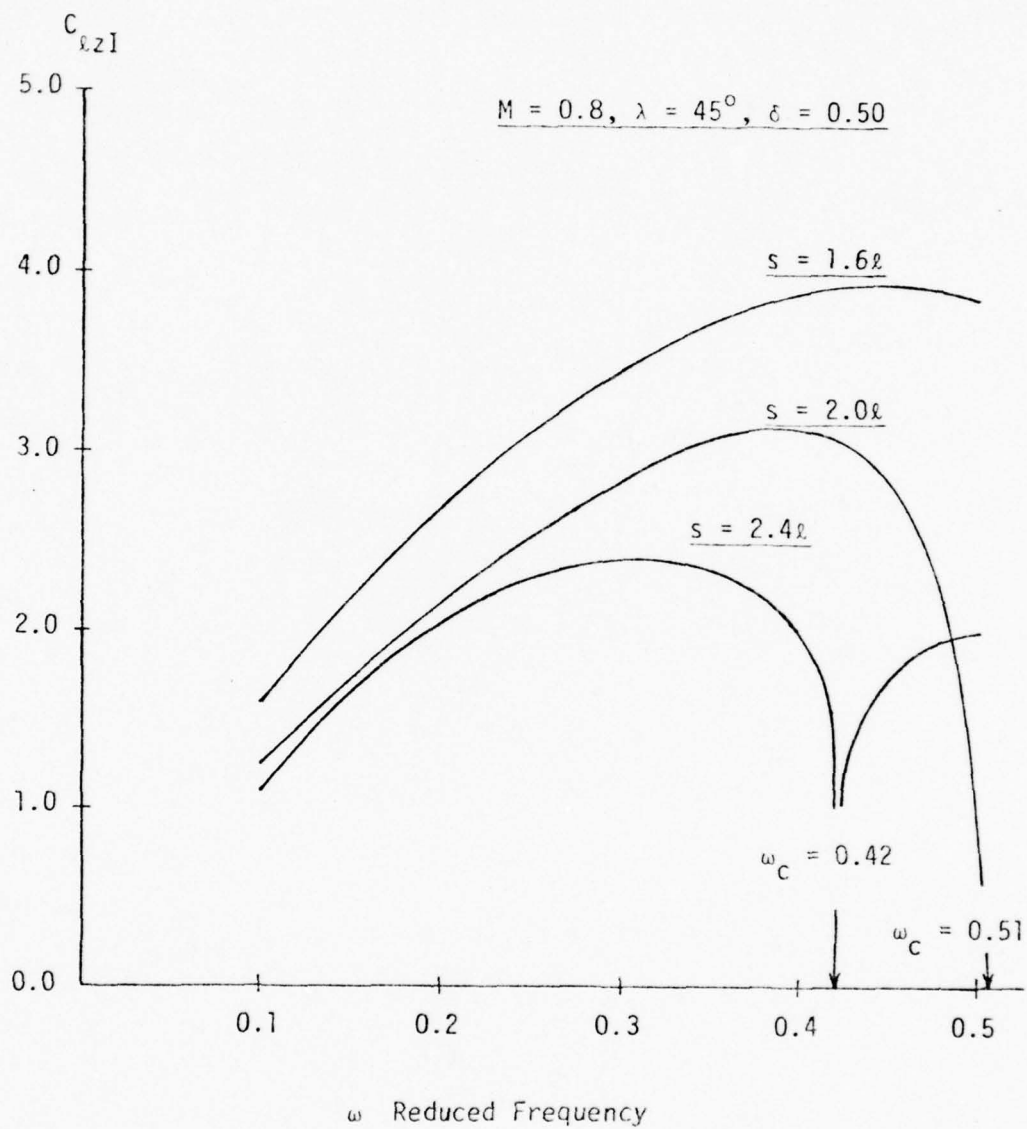


Fig. 7 Effect of Interblade Spacing on  $C_{LZI}$ .

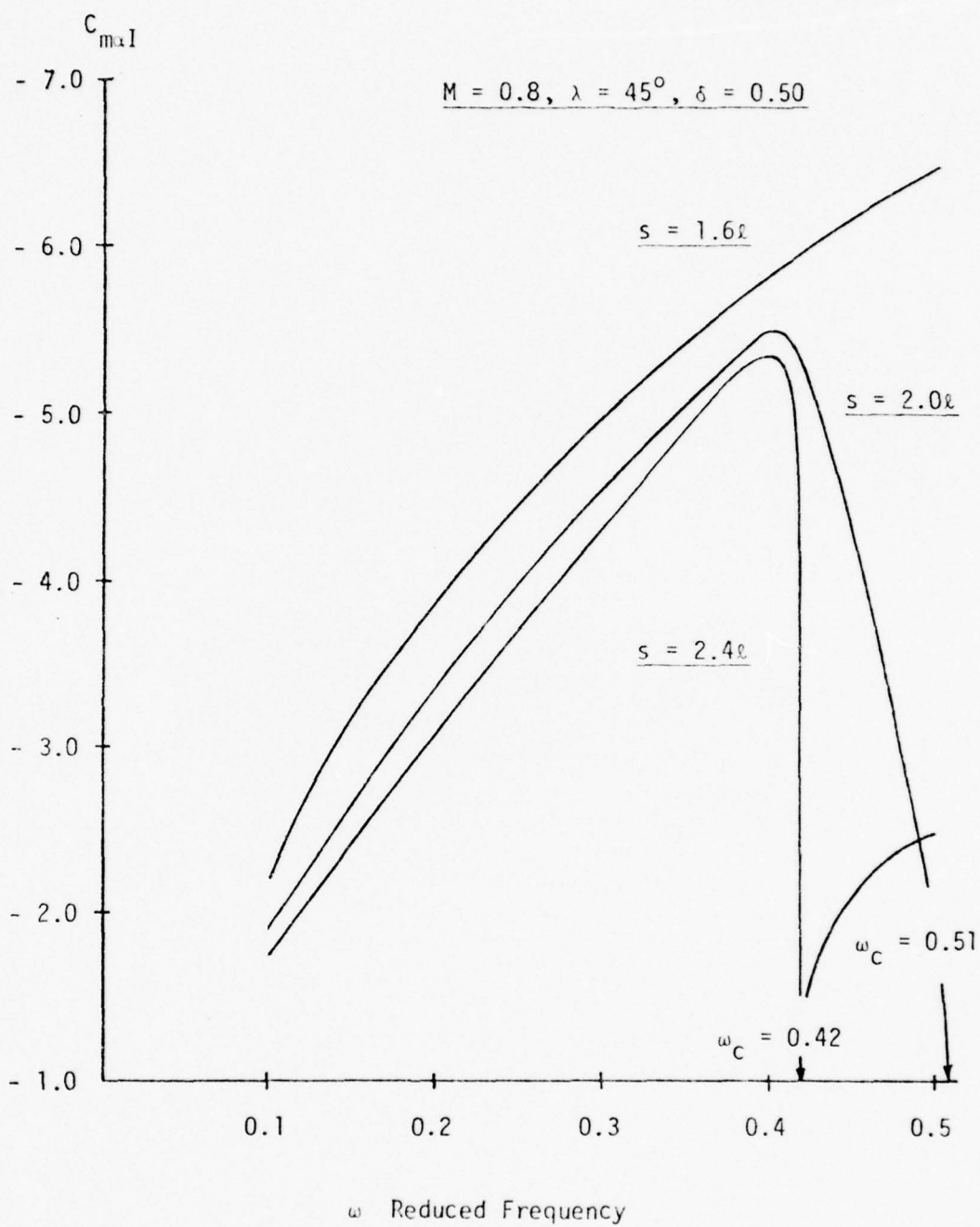


Fig. 8 Effect of Interblade Spacing on  $C_{m\alpha I}$ .

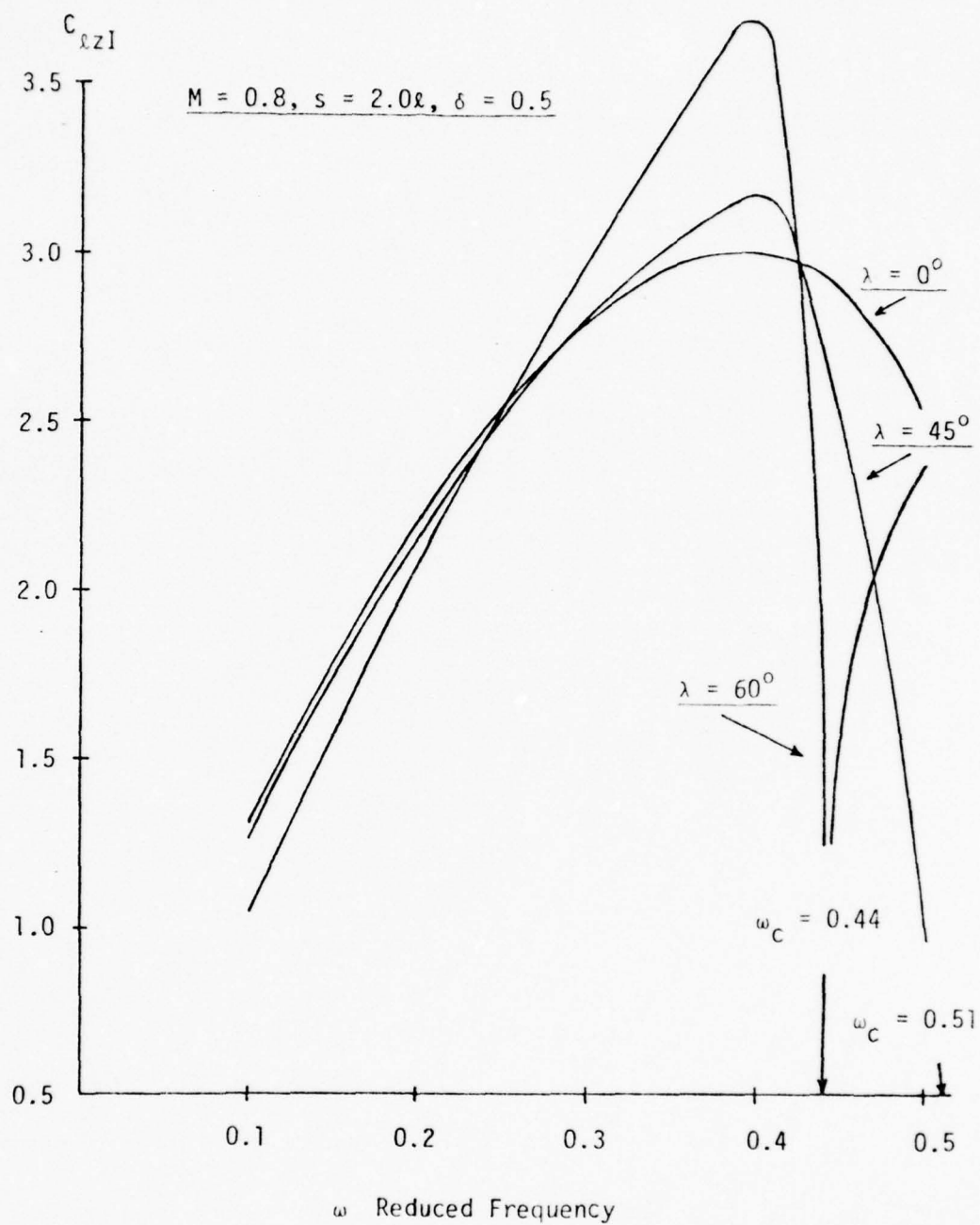


Fig. 9 Effect of Stagger Angle on  $C_{lz1}$ .

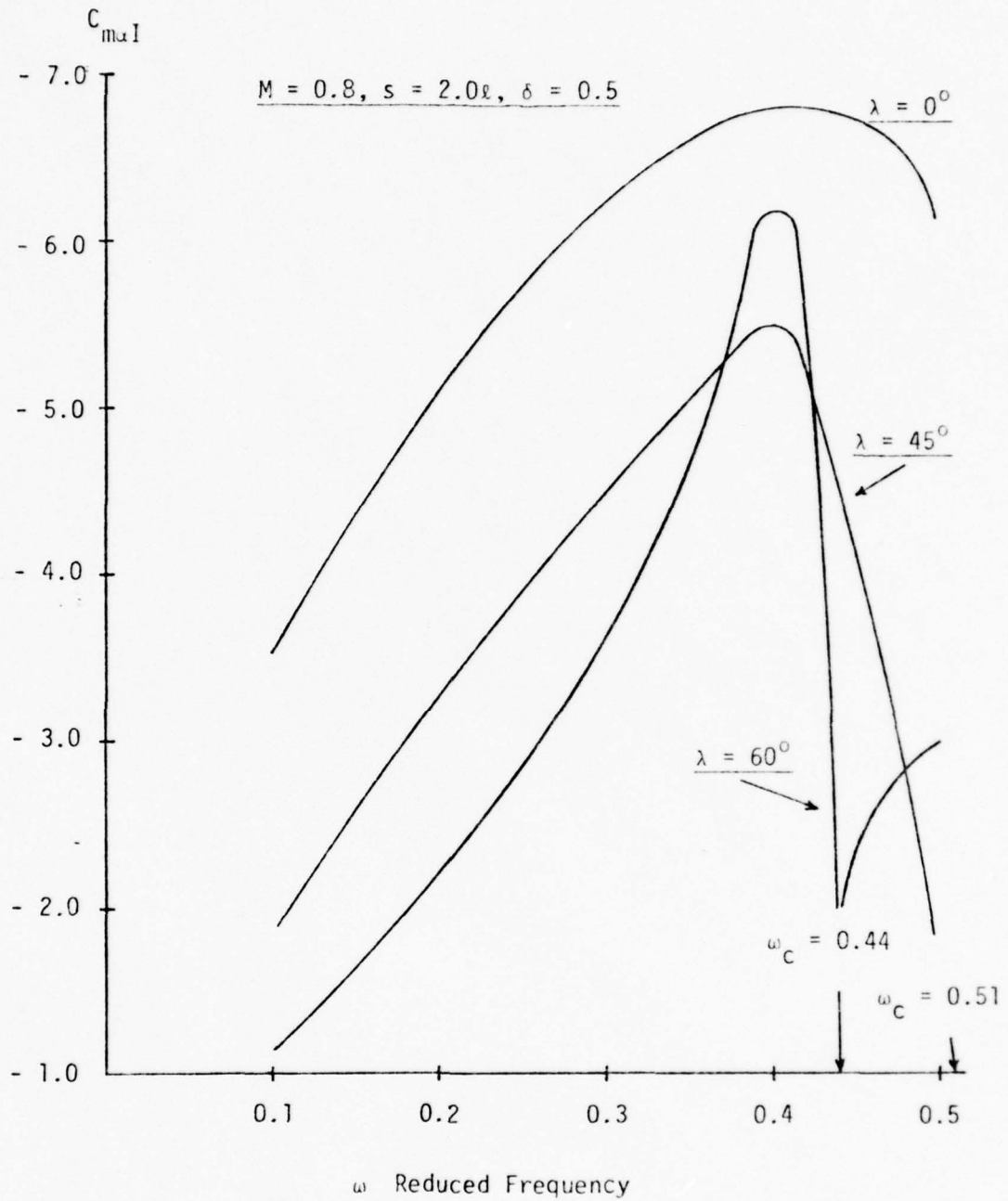


Fig. 10 Effect of Stagger Angle on  $C_{m\alpha I}$ .

are for  $\lambda = 0^\circ$ ,  $\omega_c = 1.18$ ;  $\lambda = 45^\circ$ ,  $\omega_c = 0.51$ ; and  $\lambda = 60^\circ$ ,  $\omega_c = 0.44$ .

As the stagger angle increases, the lowest critical frequency decreases. All the coefficients are presented with respect to the reference axis at mid-chord. In Ref. 7, Jones has shown that it is possible to incite pure pitching oscillation in the airfoils in cascade when  $\lambda = 0^\circ$  and  $0.73 < \omega < 0.98$  with a reference axis forward of the mid-chord. However, since the values given in Fig. 9 only consider the practical range of values for  $0.1 < \omega < 0.5$ , the translational damping coefficient  $C_{\ell z I}$  remains positive indicating that there is no pure translational instability.

Figures 11 and 12 show the effect of interblade phase lag ( $\sigma = 0^\circ$ ,  $90^\circ$ , and  $180^\circ$ ) on  $C_{\ell z I}$  and  $C_{m \alpha I}$ , respectively when  $M = 0.8$ ,  $s = 2.0\lambda$ , and  $\lambda = 45^\circ$  as  $\omega$  is varied from 0.1 to 0.5. For the parameters and the range of frequency values considered, the critical frequency for  $\sigma = 180^\circ$  is  $\omega_c = 0.51$ . The translational and pitching damping constants remain positive throughout the range of frequency values considered. However, as  $\sigma$  is increased with increasing  $\omega$ , the damping decreases rapidly for  $\sigma = 180^\circ$  until it equals zero at  $\omega = \omega_c$ .

#### Single Degree of Freedom

A single degree of freedom analysis for torsion was performed on a cascade of blades using the lifting surface theory developed by Jones and Rao. After obtaining the results, a comparison was made to the results obtained by Whitehead<sup>9</sup> who employed a technique developed by Smith<sup>17</sup> to obtain the aerodynamic forces and moments. Whitehead distinguished a region of flutter that he termed as "sub-critical flutter",

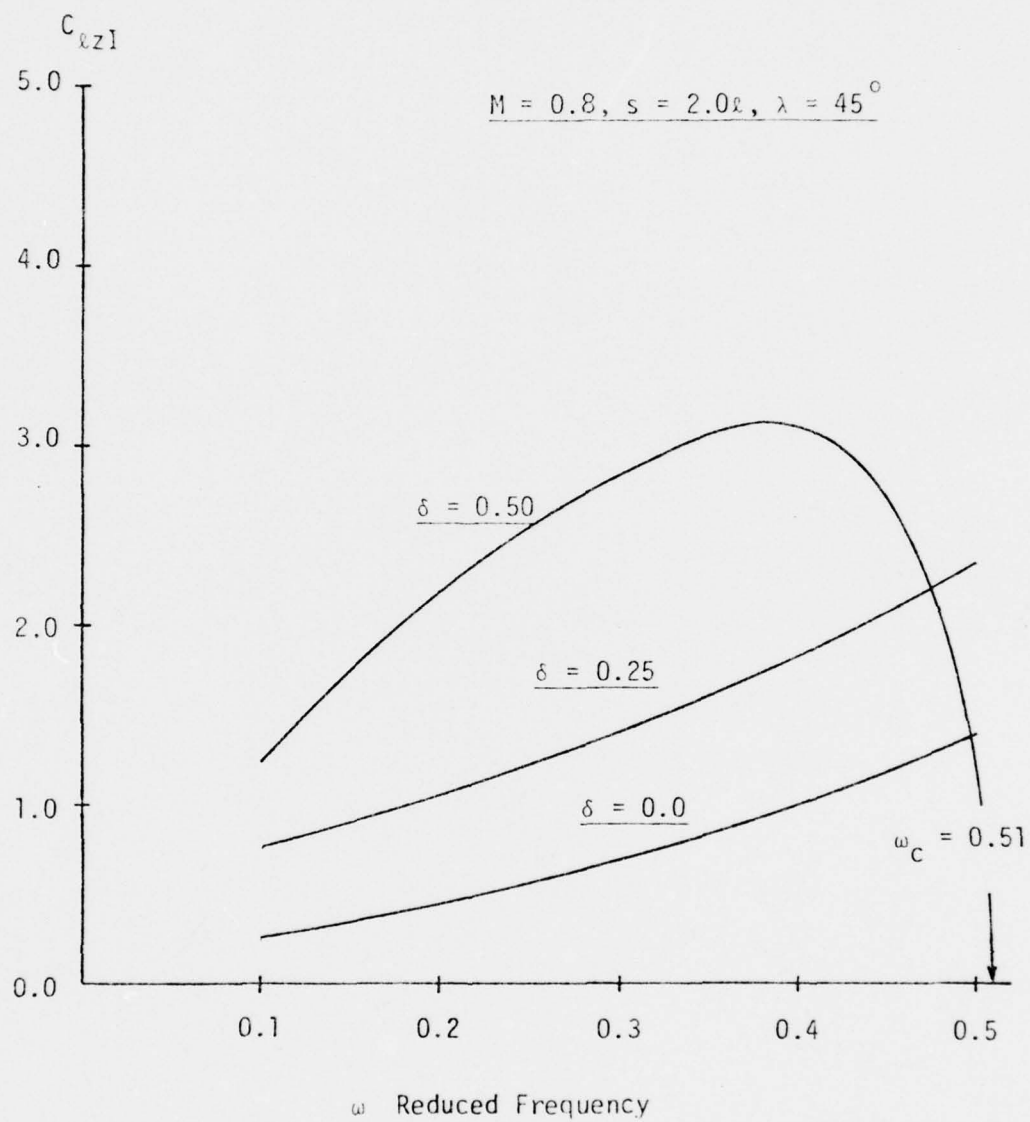


Fig. 11 Effect of Phase Lag on  $C_{lzI}$ .

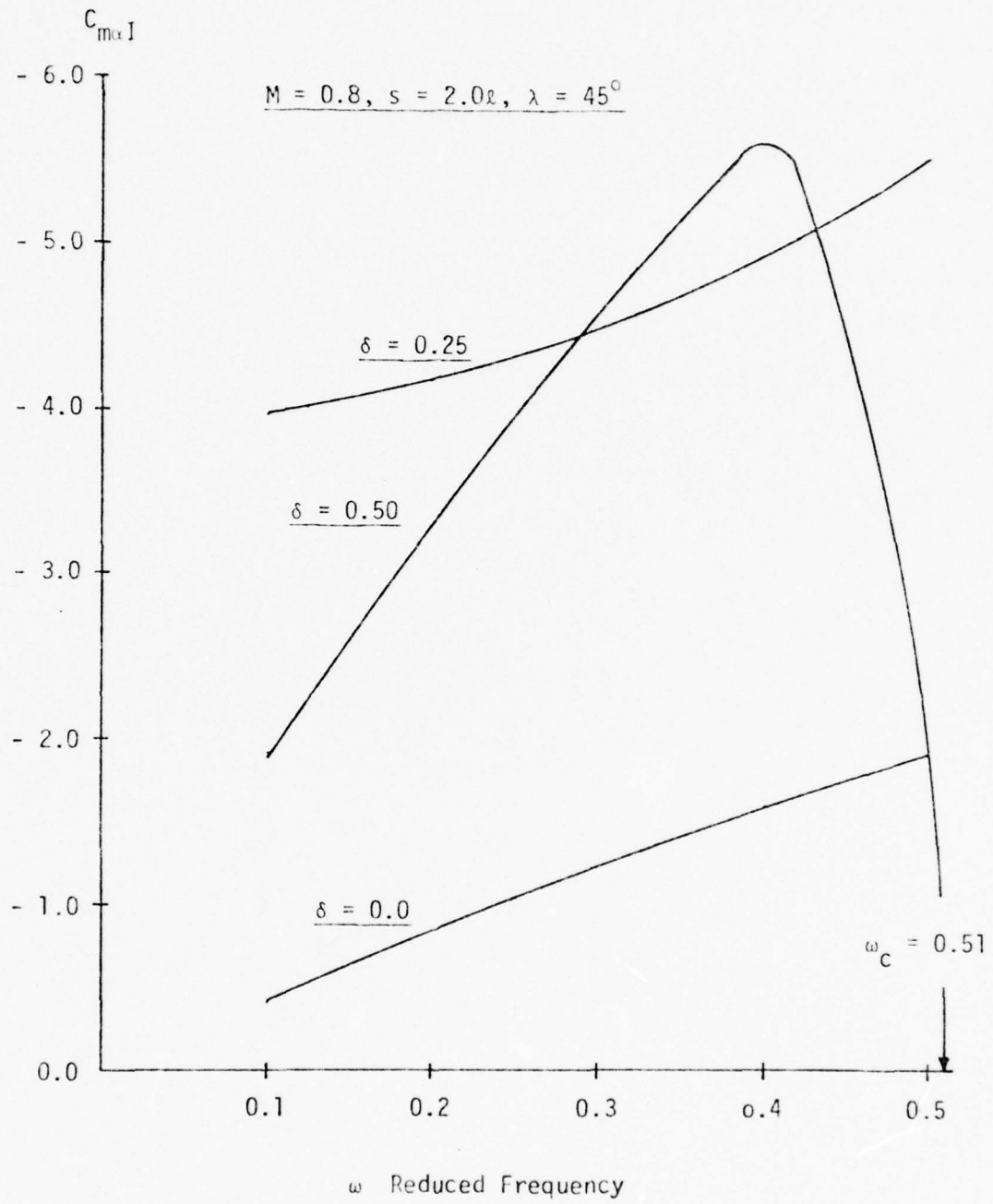


Fig. 12 Effect of Phase Lag on  $C_{m\alpha I}$ .

which occurs in a regime where any acoustic waves generated cannot propagate upstream and downstream. Figure 13 shows results that Whitehead obtained for a space-to-chord ratio of 1.0, a stagger angle of 45 degrees, a position of the torsional axis at 58.8 percent chord, and an interblade phase angle of 60 degrees. The imaginary part of the moment coefficient is plotted against the reduced frequency parameter. Also shown in Fig. 13 is a plot of the imaginary part of the moment coefficient as obtained by utilizing the Jones/Rao technique. As can be seen, when given the same conditions, the results obtained when using the Jones/Rao lifting surface technique agree closely with the results obtained by Whitehead. As shown previously, the imaginary part of the moment coefficient is capable of adding energy when it is negative. Assuming that there is no mechanical damping involved, flutter will occur as a net result of energy being added to the system. However, in reporting his results, Whitehead found that he had significant mechanical damping and had to allow for an average value as a flutter limit. This limit is shown in Fig. 13. If the value of the imaginary part of the moment coefficient is below this line, then flutter is predicted. The point where it is just possible for the flutter to exist is referred to as a flutter boundary. Whitehead observed that as the Mach number is increased, the points at which flutter is just possible move to progressively lower values of the frequency parameter. This corresponds to higher fluid velocities or to lower blade stiffness. The effect of Mach number is therefore highly significant.

Figure 14 shows the frequency parameter below which torsional flutter is just possible and has been plotted against blade axis

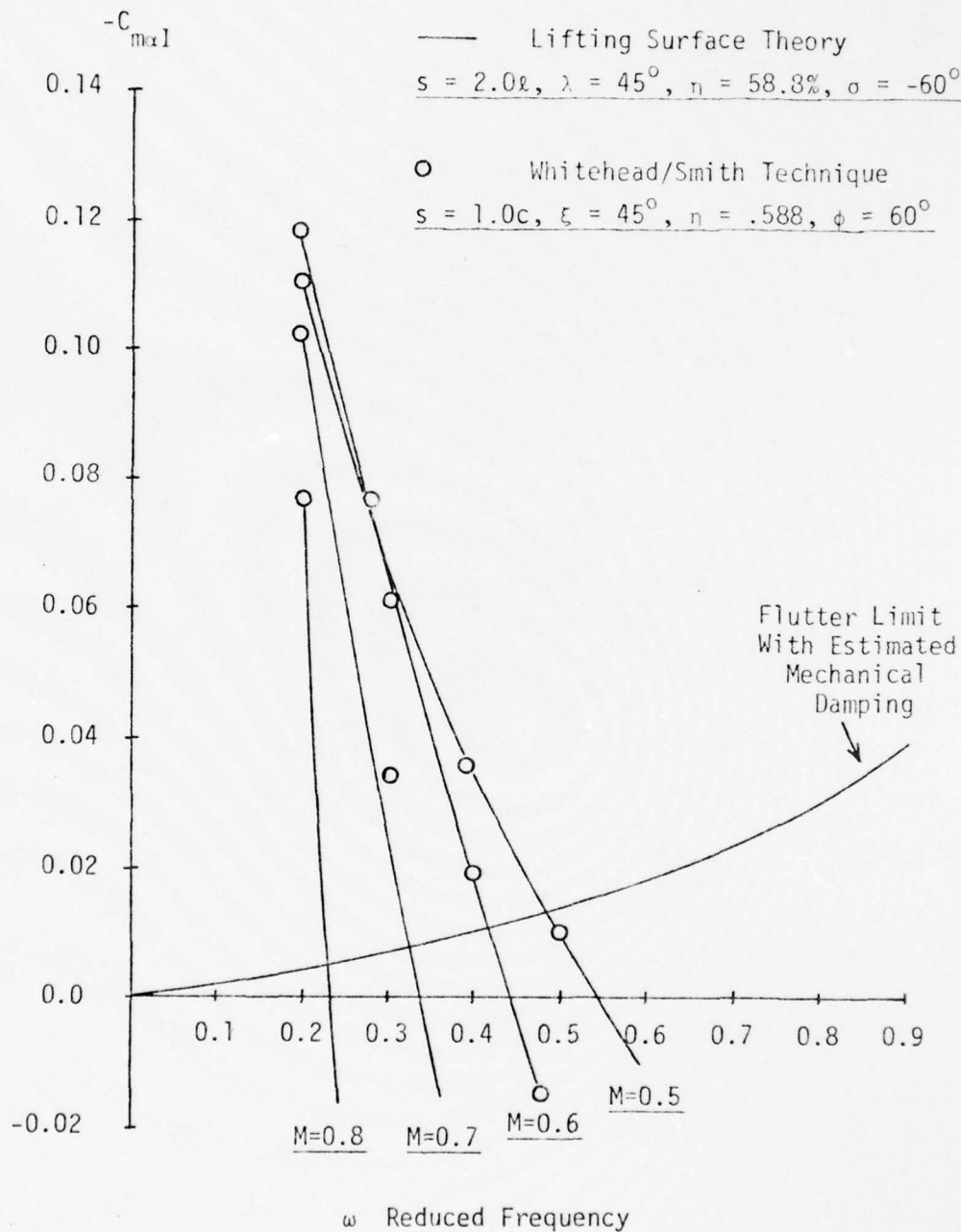


Fig. 13 Torsional Flutter Boundaries .

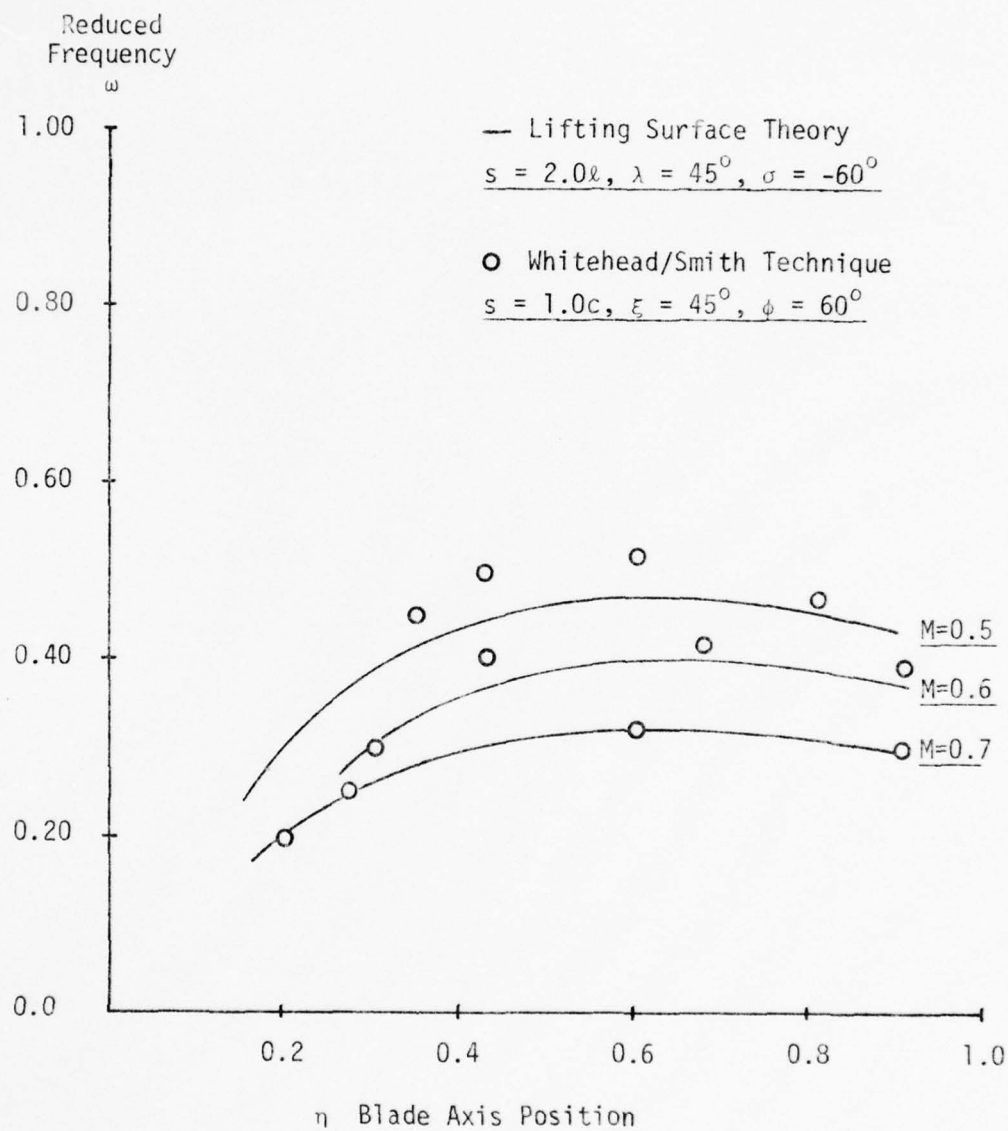


Fig. 14 Sub-Critical Flutter.

position. Once again, a comparison is made by utilizing the Jones/Rao technique and the Whitehead/Smith technique. The results are in close agreement and concur with Whitehead's observation that increasing the Mach number is favorable and that the worst position for the torsional axis is around fifty to seventy percent chord.

#### Two Degrees of Freedom

A numerical investigation for two degrees of freedom was conducted using the program for unsteady airload prediction and interfacing it with the program developed for flutter analysis. The geometrical and structural properties of the cascade reference airfoil used in this analysis were calculated from data obtained from Refs. 18, 19, and 20. These properties are given in App. B. To obtain the flutter speed and frequency, the program was executed for the given cascade according to the procedure as outlined in the block diagram of Fig. B-1 in App. B.

Figure 15 represents the results obtained for the flutter analysis for various values of interblade spacing ( $s = 1.0\lambda, 1.1\lambda, 1.2\lambda,$  and  $1.3\lambda$ ) while the interblade stagger angle was varied from 44 degrees to 60 degrees. Over the range of values considered, it can be seen from Fig. 15 that as the interblade stagger angle is increased, the flutter Mach number also increases. This indicates that an increase in the interblade stagger angle would be beneficial in preventing flutter at the lower Mach numbers. This trend is in general agreement with a report by White and Rao<sup>21</sup> in which a cascade of helicopter rotor blades was studied at various stagger angles and rotor blades spacings.

Figure 16 shows the effect of varying the interblade spacing for

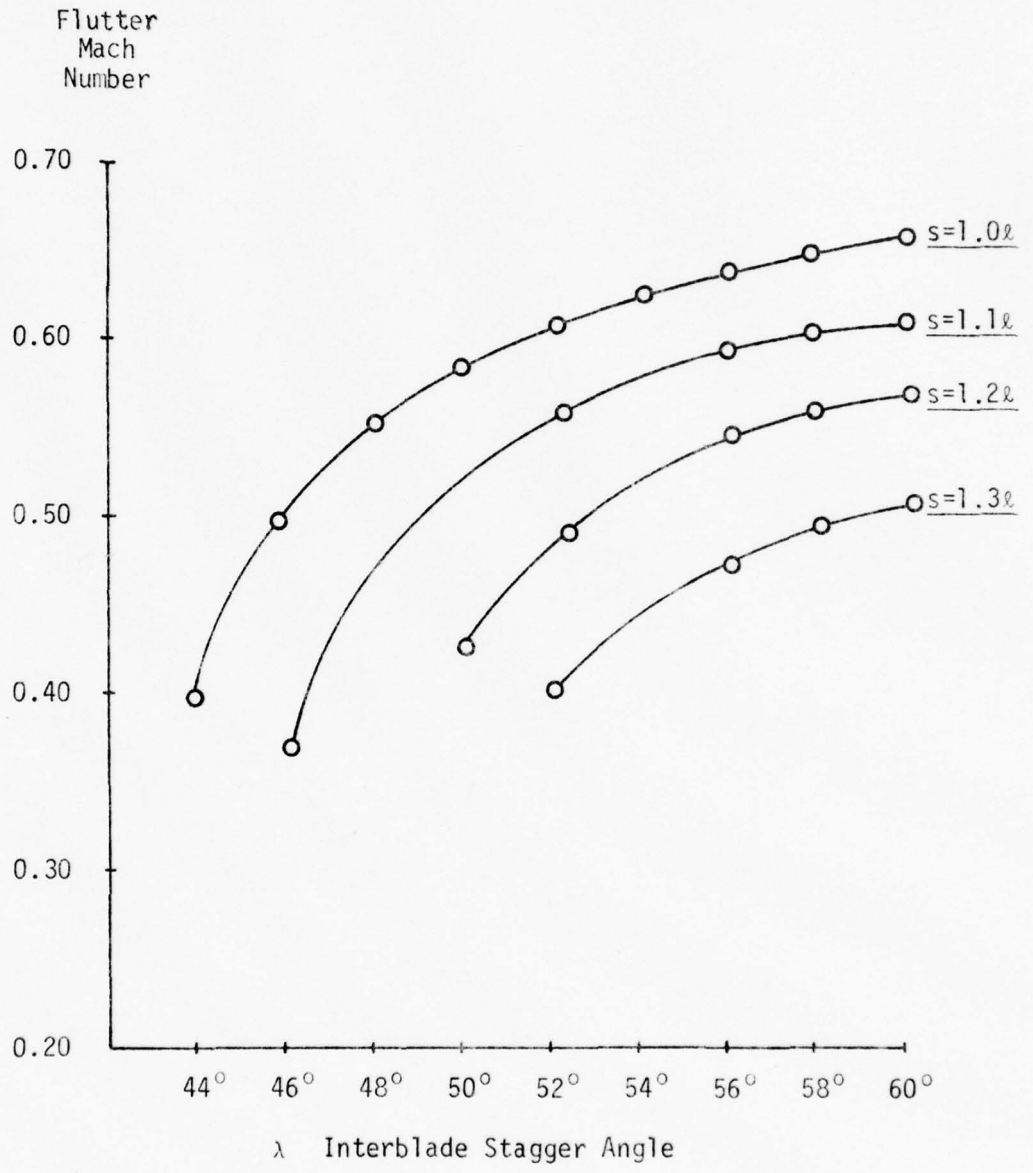


Fig. 15 Effect of Interblade Stagger Angle on Flutter Speed .

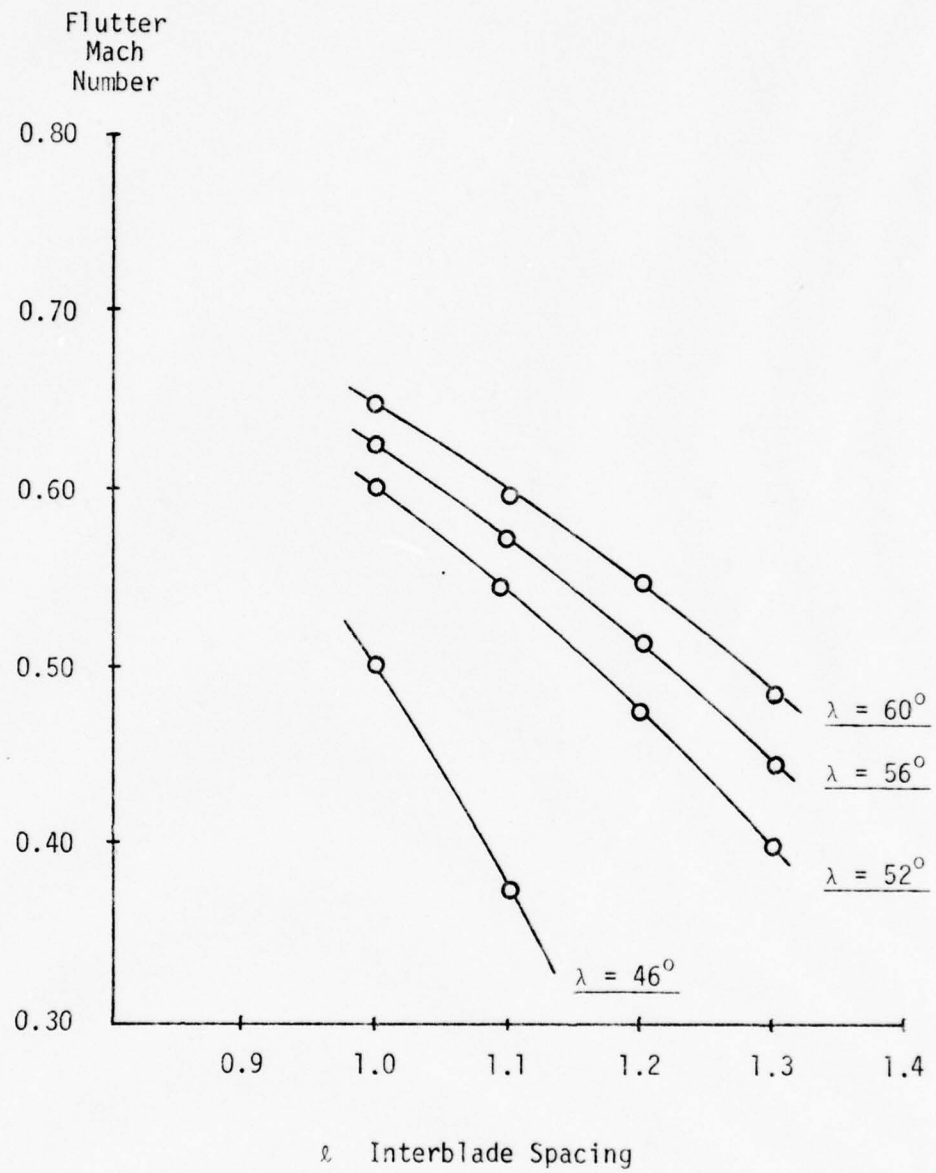


Fig. 16 Effect of Interblade Spacing on Flutter Speed .

various interblade stagger angles ( $\lambda = 46^\circ, 52^\circ, 56^\circ, \text{ and } 60^\circ$ ). The trend of the curves shows that as the interblade spacing increases for a given interblade stagger angle, the flutter Mach speed decreases. This indicates that increasing the interblade spacing will have a destabilizing effect on the cascade of blades. This same trend was also observed by White and Rao in their work with helicopter rotor blades.

A summary of the results of the two degree of freedom flutter analysis is presented in Table 3.

Table 3 Summary of Two Degree of Freedom Flutter Analysis

Interblade Stagger Angle $\lambda$ (Degrees)	Interblade Spacing $s$	Flutter Mach Number $M$	Flutter Reduced Frequency $\omega$	Interblade Phase Lag $\sigma$ (Degrees)
44	1.0 $l$	0.4087	0.4539	-30
46	1.0 $l$	0.5028	0.3671	-30
48	1.0 $l$	0.5497	0.3347	-30
50	1.0 $l$	0.5676	0.3234	-30
54	1.0 $l$	0.6109	0.2988	-30
55	1.0 $l$	0.6216	0.2935	-30
56	1.0 $l$	0.6300	0.2888	-30
60	1.0 $l$	0.6445	0.2809	-30
46	1.1 $l$	0.3783	0.4907	-30
52	1.1 $l$	0.5561	0.3301	-30
56	1.1 $l$	0.5843	0.3128	-30
58	1.1 $l$	0.5818	0.3138	-30
60	1.1 $l$	0.6058	0.3001	-30
50	1.2 $l$	0.4300	0.4305	-30
52	1.2 $l$	0.4809	0.3837	-30
56	1.2 $l$	0.5336	0.3440	-30
58	1.2 $l$	0.5406	0.3390	-30
60	1.2 $l$	0.5501	0.3325	-30
52	1.3 $l$	0.4045	0.4580	-30
56	1.3 $l$	0.4715	0.3911	-30
58	1.3 $l$	0.4757	0.3872	-30
60	1.3 $l$	0.4990	0.3682	-30

## CONCLUSIONS AND RECOMMENDATIONS

A unique velocity potential lifting surface technique has been used to determine the unsteady airloads for an infinite cascade of staggered blades in subsonic flow. The unsteady airloads were then utilized in a FORTRAN program to perform a flutter analysis for a single degree of freedom system in torsion and for a two degree of freedom system in bending and torsion.

Several geometric and flow parameters of a staggered cascade were varied over a specific range of values and were found to influence the cascade in the following manner:

1. If Mach number is increased, it will have an increased damping effect on the stability of the cascade in pitching motions.
2. If interblade spacing is increased, the damping decreases while still below the first critical frequency and is equal to zero at the first critical frequency.
3. As interblade stagger angle increases, the lowest critical frequency decreases.
4. As interblade phase lag is increased with increasing reduced frequency, the damping will decrease rapidly to zero for an interblade phase lag of 180 degrees.

When the cascade was analyzed for a single degree of freedom system in torsion, results were found to compare favorably with the results obtained by D.S. Whitehead<sup>9</sup> for flutter boundaries. A comparison of the lifting surface technique employed by Rao and Jones<sup>8</sup> and a different technique utilized by Whitehead in determining torsional flutter, were

shown to be in agreement in indicating that increasing Mach number is a desirable condition.

By utilizing work performed by Rao<sup>16</sup> and White and Rao<sup>21</sup>, a FORTRAN program was developed that is capable of determining the flutter speed and frequency of a staggered cascade of blades in unsteady subsonic flow. This program is valid for a two degree of freedom system in bending and torsion. It was determined that increasing interblade stagger angle would be beneficial in preventing flutter at low Mach numbers while an increase in interblade spacing would be a destabilizing influence on the cascade of blades.

While a new flutter program was developed to determine the cascade flutter speed and frequency, only a limited range of values were analyzed when varying cascade parameters. This was due primarily to the iterative scheme that was involved and the associated expense of computer computational time. Even though cost effectiveness was considered as a criterion in the development of this program, the program still remains as being a reasonably efficient technique to be used in determining the unsteady aerodynamic derivatives, the flutter speed, and the flutter frequency for a given cascade. By way of example, the run time associated with determining the flutter speed and frequency for the example given in App. B, utilized less than twelve seconds of CPU execution time on the AMDAHL 470V/6 computer at Texas A&M University. However, further improvements could be made in the overall efficiency of the program and the iterative procedure it utilizes. Additionally, investigation should also be conducted over a larger range of cascade parameter values to determine their effect on the cascade flutter speeds and frequencies.

## REFERENCES

<sup>1</sup>Whitehead, D.S., "Bending Flutter of Unstalled Cascade Blades at Finite Deflection," British Aeronautical Research Council, R&M 3386, October 1962.

<sup>2</sup>Kemp, N.H., and Sears, W.R., "The Unsteady Forces Due to Viscous Wakes in Turbomachines," Journal of Aeronautical Sciences, Vol. 22, 1955, pp. 478-483.

<sup>3</sup>Schorr, B., and Reddy, K.C., "Inviscid Flow Through Cascades in Oscillatory and Distorted Flow," AIAA Journal, Vol. 9, No. 11, October 1971, pp. 2043-2050.

<sup>4</sup>Jones, W.P., and Moore, J.A., "Flow in the Wake of a Cascade of Oscillating Airfoils," AIAA Journal, Vol. 10, No. 12, December 1972, pp. 1600-1605.

<sup>5</sup>Rao, B.M., and Jones, W.P., "Unsteady Airloads on a Cascade of Staggered Blades in Incompressible Flow," Presented at the workshop on unsteady flows in jet engines, United Aircraft Research Laboratories, July 1974.

<sup>6</sup>Fleeter, S., "Fluctuating Lift and Moment Coefficients for Cascaded Airfoils in a Nonuniform Compressible Flow," Journal of Aircraft, Vol. 10, No. 2, February 1973, pp. 93-98.

<sup>7</sup>Jones, W.P., and Moore, J.A., "Aerodynamic Theory for a Cascade of Oscillating Airfoils in Compressible Subsonic Flow," Texas A&M University, TEES-3068-75-01, February 1975.

<sup>8</sup>Rao, B.M., and Jones, W.P., "Unsteady Airloads on a Cascade of Staggered Blades in Subsonic Flow," Presented at the forty-sixth propulsion energetics panel meeting, Advisory Group for Aerospace Research and Development, September 1975.

<sup>9</sup>Whitehead, D.S., "The Effect of Compressibility on Unstalled Torsional Flutter," British Aeronautical Research Council, R&M 3754, August 1973.

<sup>10</sup>Scanlan, R.H., and Rosenbaum, R., "Aircraft and Vibration," Dover Publications, Inc., New York, 1951.

<sup>11</sup>Ashley, H., and Landahl, M.T., Aerodynamics of Wings and Bodies, Addison-Wesley Publishing Co., Inc., Reading, Massachusetts, 1965.

<sup>12</sup>Jones, W.P., "Notes on Unsteady Aerodynamics," Unpublished notebook, Department of Aerospace Engineering, Texas A&M University, February 1975.

<sup>13</sup>Infeld, L., Smith, V.G., and Chien, W.Z., "On Some Series of Bessel Functions," Journal of Mathematics and Physics, Vol. XXVI, No. 1, April 1947, pp. 22-28.

<sup>14</sup>Kaji, S., and Okazaki, T., "Propagation of Sound Waves Through a Blade Row," Journal of Sound and Vibration, Vol. 11, No. 3, 1970, Parts I and II, pp. 339-375.

<sup>15</sup>Bisplinghoff, R.L., Ashley, H., and Halfman, R.L., Aeroelasticity, Addison-Wesley Publishing Co., Inc., Reading, Massachusetts, 1957.

<sup>16</sup>Rao, B.M., "Unsteady Airloads on a Cascade of Staggered Blades in Subsonic Flow," Computer program developed at Texas A&M University, September 1975.

<sup>17</sup>Smith, S.N., "Discrete Frequency Sound Generation in Axial Flow Turbomachines," British Aeronautical Research Council, R&M 3709, 1972.

<sup>18</sup>Sawyer, J.W., "Gas Turbine Engineering Handbook," Gas Turbine Publications, Inc., Stamford, Connecticut, 1966.

<sup>19</sup>Emery, J.C., "Systematic Two-Dimensional Cascade Tests of NACA 65-Series Compressor Blades at Low Speeds," NACA TR-1368, U.S. Government Printing Office, 1969.

<sup>20</sup>Johnson, I.A., and Bullock, R.O., "Aerodynamic Design of Axial-Flow Compressors," NASA SP-36, National Aeronautics and Space Administration, Washington, D.C., 1965.

<sup>21</sup>White, G.P., and Rao, B.M., "Flutter Analysis of a Cascade of Rotor Blades," Air Force Research Project Report AROSR-74-2700B, 1977.

## APPENDIX A

## Physical Interpretation of Resonance Conditions

Consider the airfoil as given below in Fig. A-1,

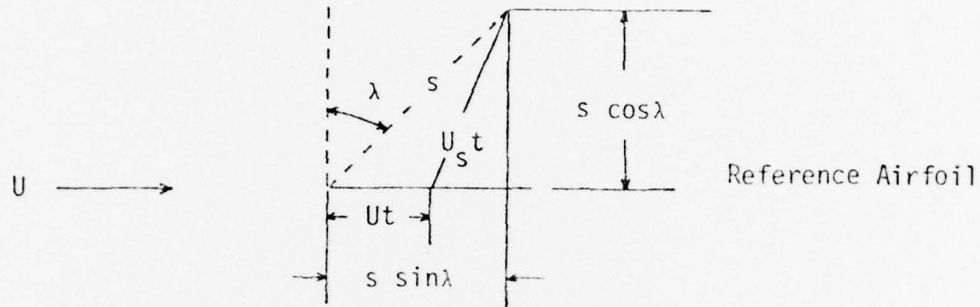


Fig. A-1 Resonance Model .

where  $\lambda$  is stagger angle,  $s$  is the distance between the leading edge of consecutive airfoils, and  $U$  is freestream velocity. The influence created by the unsteady motion of the airfoil will propagate and influence the reference airfoil after time  $t$ . This gives,

$$[U_s t]^2 = [s(\sin \lambda) - Ut]^2 + [s(\cos \lambda)]^2 \quad (A1)$$

$$U_s^2 t^2 = s^2(\sin^2 \lambda) - 2Ut s(\sin \lambda) + U^2 t^2 + s^2(\cos^2 \lambda) \quad (A2)$$

$$[U_s^2 - U^2] t^2 + [2Us(\sin \lambda)] t - s^2 = 0 \quad (A3)$$

solving for  $t$  gives,

$$t = -\frac{Us(\sin \lambda)}{(U_s^2 - U^2)} \pm \frac{\sqrt{U^2 s^2(\sin^2 \lambda) + s^2(U_s^2 - U^2)}}{(U_s^2 - U^2)} \quad (A4)$$

given that  $\beta = [1 - M_\infty^2]^{1/2}$  and  $M_\infty = \frac{U}{U_s}$ , Eq. (A4) becomes,

$$t = -\frac{M^2}{\beta^2} \frac{S}{U} (\sin \lambda) \pm \frac{M^2}{\beta^2} \frac{S}{U} \sqrt{\sin^2 \lambda + \left(\frac{1}{M^2} - 1\right)}. \quad (\text{A5})$$

From Ref. 7, it is shown that,

$$pt + \sigma = 0, 2\pi, \text{ etc.}, \quad (\text{A6})$$

where  $p (= \frac{\omega U}{l})$  is the frequency of blade oscillation in rad/sec, and  $\sigma$  is phase lag. Now Eq. (A5) becomes,

$$-\sigma = -\frac{M^2}{\beta^2} \omega S (\sin \lambda) \pm \frac{M^2}{\beta^2} \omega S \sqrt{\sin^2 \lambda + \left(\frac{1}{M^2} - 1\right)} \quad (\text{A7})$$

where  $S (= \frac{S}{l})$  is space to blade semi-chord ratio. After consolidating terms, Eq. (A7) becomes,

$$\frac{\omega S}{\sigma} = \pm \sqrt{\frac{1}{M^2} - \cos^2 \lambda} - \sin \lambda. \quad (\text{A8})$$

The critical or resonance frequency is then given as,

$$\omega_c = \left[ \pm \sqrt{\frac{1}{M^2} - \cos^2 \lambda} - \sin \lambda \right] \frac{\sigma}{S}. \quad (\text{A9})$$

## APPENDIX B

## Example Problem for Two Degree of Freedom Flutter

A numerical test case for cascaded airfoil flutter analysis was computed using a flutter analysis FORTRAN program interfaced with the unsteady airload prediction program. The geometrical and structural properties of the reference airfoil used in this analysis are calculated from data obtained from Refs. 18, 19, and 20, and are given below.

Static moment about the elastic axis	$S = 5.35 \times 10^{-4}$ slug-ft.
Moment of inertia about elastic axis	$I = 6.316 \times 10^{-5}$ slug-ft <sup>2</sup> .
Mass per unit span of blade	$M = 0.0214$ slugs/ft.
Bending natural frequency	$\omega_z = 1000$ rad/sec.
Torsional natural frequency	$\omega_\alpha = 2000$ rad/sec.

The cascade parameters used are,

Blade semi-chord length	$\ell = 0.0833$ ft.
Interblade spacing	$s = 1.2\ell$
Interblade phase lag	$\delta = -0.0835$
Interblade stagger angle	$\lambda = 52$ deg.

To obtain the flutter speed and frequency, the program was executed for the given cascade according to the procedure as given in the block diagram of Fig. B-1. After the input parameters are read into the program and initial values are assumed for the Mach number and the reduced

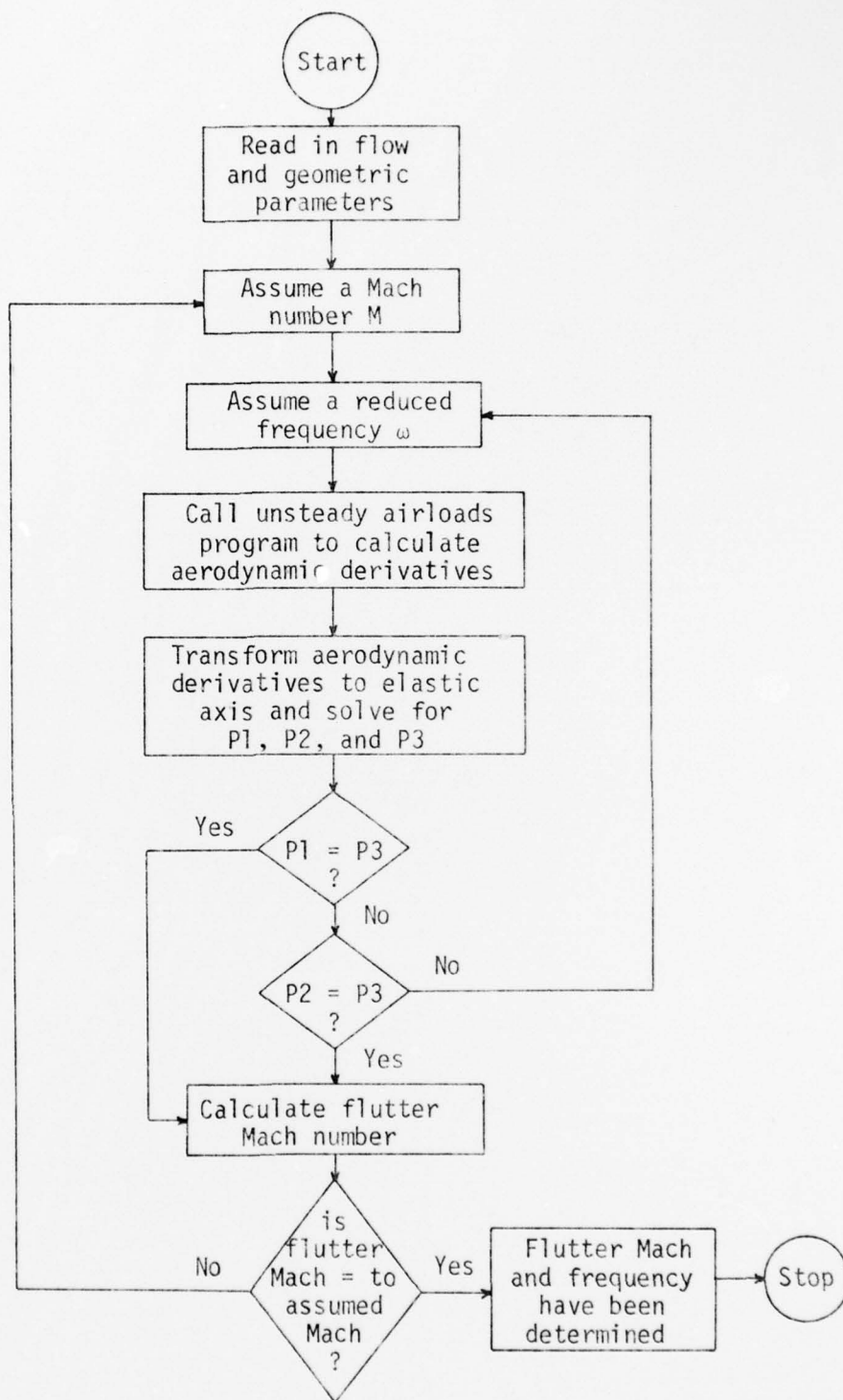


Fig. B-1 Program Flowchart .

frequency, the program calculates the unsteady aerodynamic derivatives that are to be used as the forcing functions in Lagrange's equations of motion. The aerodynamic derivatives that are initially obtained are referred to the blade mid-chord axis. Since it is necessary for the aerodynamic derivatives to be referred to the elastic axis, a coordinate transformation is performed as explained in App. C. After the coordinate transformation, the flutter determinant is solved. This yields P1 and P2 as solutions to the quadratic equation of the real part of the flutter determinant and P3 as a solution to the linear equation of the imaginary part of the flutter determinant. Since an iterative scheme is involved in obtaining the flutter speed and frequency, initial values of Mach number and reduced frequency are assumed. The initial values of Mach number are 0.500 and 0.5100. Several values of  $\omega$  are then calculated for each Mach number and the respective values of P1, P2, and P3 are found. These values are then plotted as shown in Fig. B-2. Figure B-2 indicates that P2 is equal to P3 when  $\omega = 0.3600$  for  $M = 0.500$  and Fig. B-3 shows that P2 is equal to P3 when  $\omega = 0.3486$  for  $M = 0.510$ . These values represent possible flutter frequencies if the assumed Mach number is equal to the flutter Mach number. When the assumed Mach number is equal to 0.500, Fig. B-2 shows  $P2 = P3 = 2293$  at  $\omega = 0.3600$ . If these values are used in the following equation,

$$M = \frac{p\ell}{\omega a} \quad (B1)$$

where  $a = 1037.26$  ft/sec. , then the flutter Mach number should be equal to 0.5116. However, since this is not equal to the assumed Mach number of 0.500, another iteration must be performed. The next iteration for an assumed Mach number of 0.510 is shown in Fig. B-3. Here it can

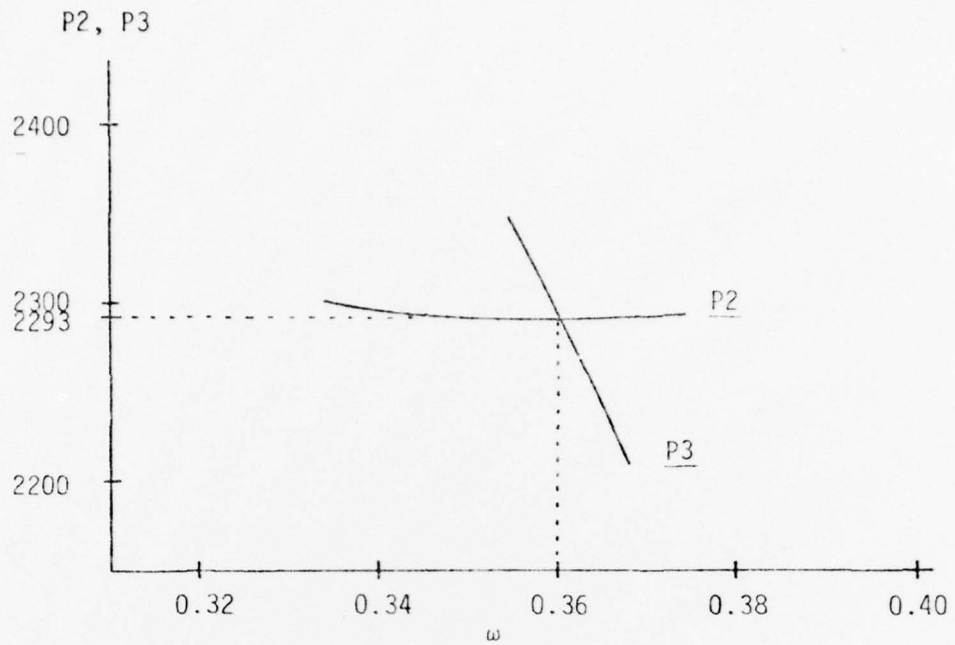


Fig. B-2 First Iteration, Mach = 0.500 .

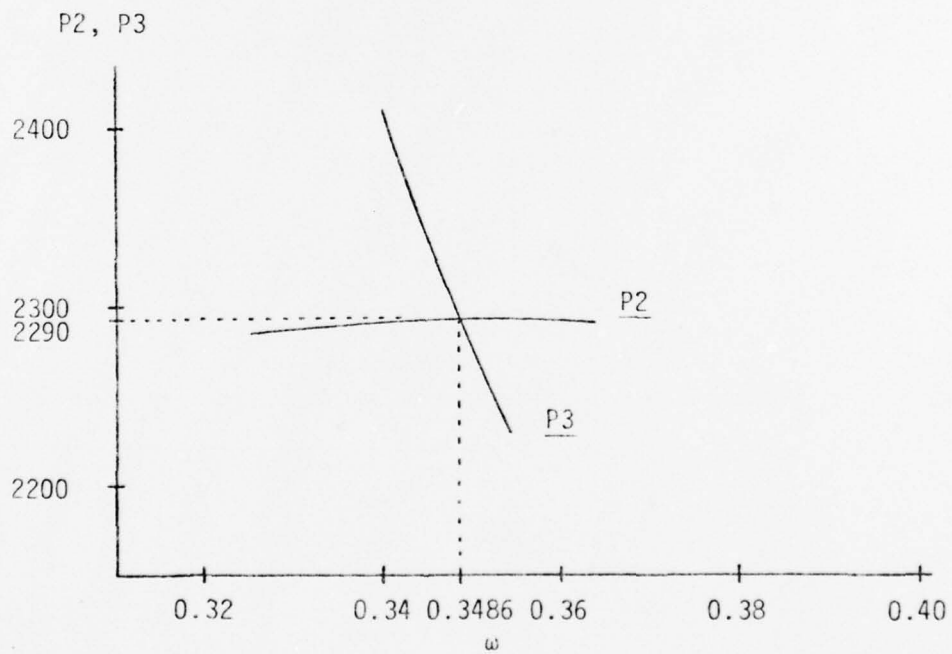


Fig. B-3 Second Iteration, Mach = 0.510 .

be seen that  $P_2 = P_3 = 2290$  at  $\omega = 0.3486$ . Again, using Eq. (B1), the flutter Mach number is calculated to be 0.5276. Once again, the calculated Mach number is not equal to the assumed Mach number, so a flutter speed still has not been determined. For the next Mach iteration, Fig. B-4 will provide the assumed Mach number. If the previous assumed Mach numbers are plotted versus the calculated flutter Mach numbers, it can be seen from Fig. B-4 that an extrapolated value of  $M = 0.480$  should be used for the next assumed Mach iteration. If this is done, then  $P_2 = P_3 = 2297$  at  $\omega = 0.3837$ . Using Eq. (B1), a calculated flutter Mach number value of  $M = 0.4809$  is obtained. Since this value is essentially the same as the assumed Mach number, it is therefore considered a valid flutter speed at a flutter frequency of  $\omega_f = 0.3837$ .

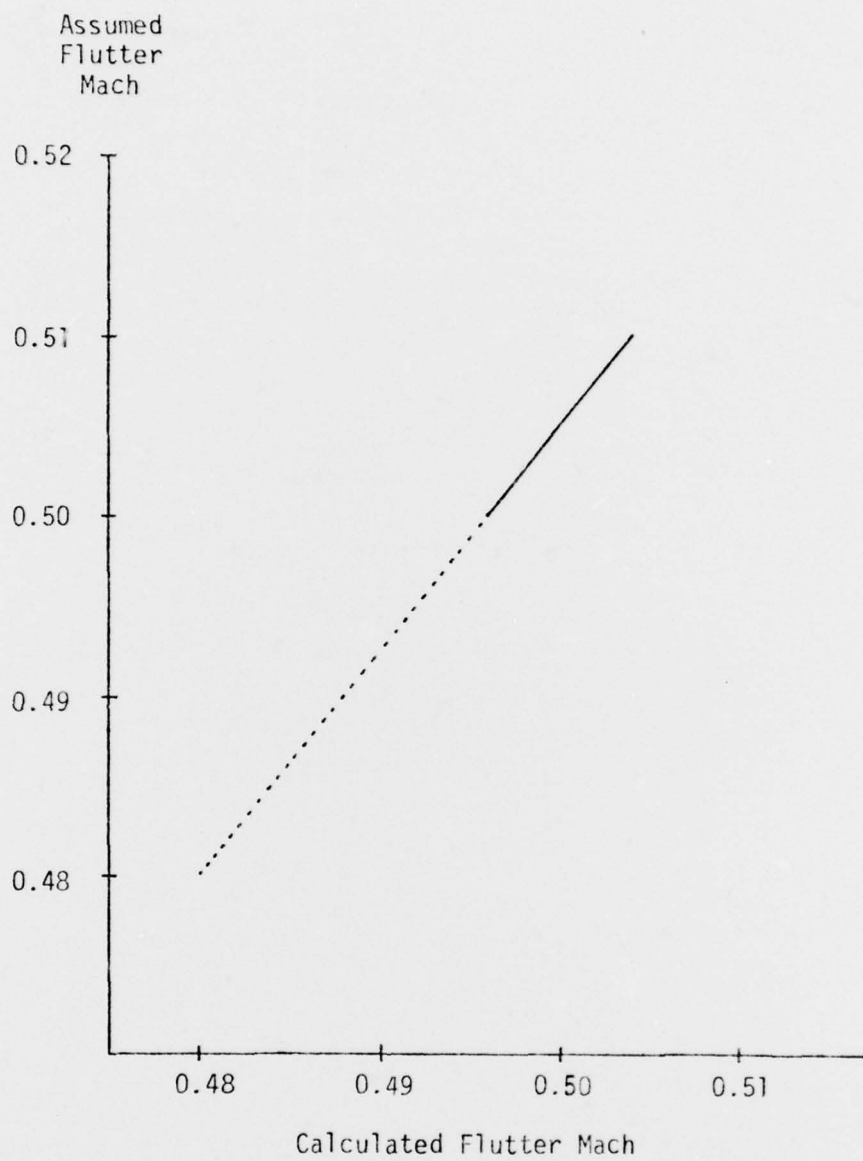


Fig. B-4 Assumed Flutter Mach Prediction .

## APPENDIX C

## Change of Reference Axis

Jones<sup>12</sup> has given a convenient axis transformation. In Fig. C-1, let the reference axis be moved from mid-chord to a point  $O'$ , at a distance  $h\ell$  forward of mid-chord.

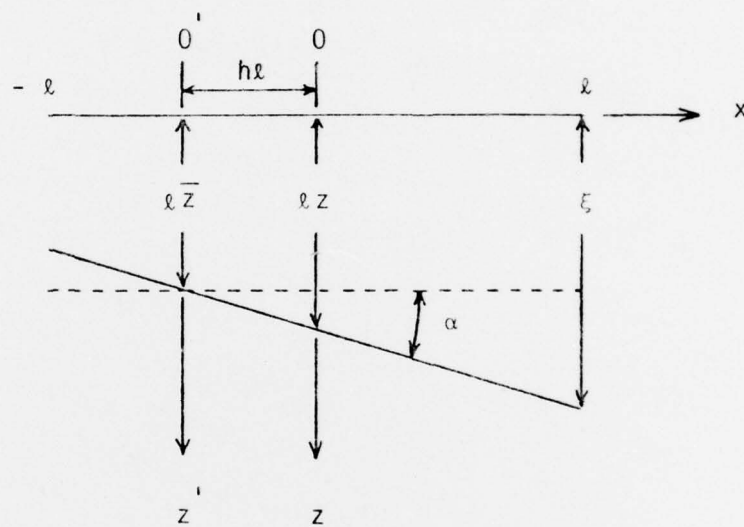


Fig. C-1 Blade Reference Axis.

When referred to the original coordinates  $z$  and  $\alpha$ , the displacement of a point,  $p$ , downwards is,

$$z = \ell z + \ell \xi \alpha + \ell(z + \xi \alpha) \quad (C1)$$

and for the new coordinates  $\bar{z}$  and  $\alpha$  referred to  $O'$ ,

$$z = \ell \bar{z} + \ell(\xi + h)\alpha \quad (C2)$$

hence,

$$z = \bar{z} + h\alpha \quad (C3a)$$

$$\alpha = \bar{\alpha} \quad (C3b)$$

If  $L$  and  $M$  are the lift and moment referred to  $O$  (mid-chord) and  $\bar{L}$  and  $\bar{M}$  are the corresponding force and moment referred to  $O'$ , it can be shown that the relation exists as shown in Fig. C-2.

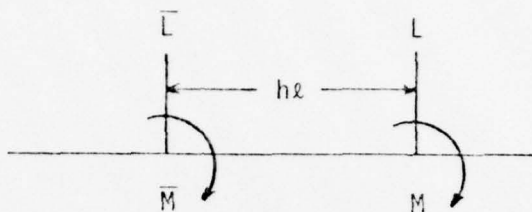


Fig. C-2 Force and Moment Orientation.

From Fig. C-2,

$$\bar{L} = L \quad (C4a)$$

$$\bar{M} = M - h\ell L \quad (C4b)$$

where  $M$  and  $\bar{M}$  are positive in the clockwise direction. It can be shown that,

$$\frac{\bar{L}}{\rho U^2 \ell} = \frac{L}{\rho U^2 \ell} = (C_{\ell z R} + i\omega C_{\ell z I})z + (C_{\ell \alpha R} + i\omega C_{\ell \alpha I})\alpha \quad (C5a)$$

$$= (C_{\ell z R} + i\omega C_{\ell z I})(\bar{z} + h\alpha) + (C_{\ell \alpha R} + i\omega C_{\ell \alpha I})\bar{\alpha} \quad (C5b)$$

$$= (\bar{C}_{\ell z R} + i\omega \bar{C}_{\ell z I})\bar{z} + (\bar{C}_{\ell \alpha R} + i\omega \bar{C}_{\ell \alpha I})\bar{\alpha} \quad (C5c)$$

Similarly,

$$\frac{\bar{M}}{\rho U^2 \ell^2} = (\bar{C}_{m z R} + i\omega \bar{C}_{m z I})\bar{z} + (\bar{C}_{m \alpha R} + i\omega \bar{C}_{m \alpha I})\bar{\alpha} \quad (C6)$$

From Eqs. (C5c) and (C6), the expressions for the new aerodynamic derivatives are given in terms of the original ones referred to the mid-chord. These equations are given as,

$$\bar{C}_{\ell zR} = C_{\ell zR} \quad (C7a)$$

$$\bar{C}_{\ell zI} = C_{\ell zI} \quad (C7b)$$

$$\bar{C}_{\ell\alpha R} = C_{\ell\alpha R} - hC_{\ell zR} \quad (C7c)$$

$$\bar{C}_{\ell\alpha I} = C_{\ell\alpha I} - hC_{\ell zI} \quad (C7d)$$

$$\bar{C}_{mzR} = C_{mzR} + hC_{\ell zR} \quad (C7e)$$

$$\bar{C}_{mzI} = C_{mzI} + hC_{\ell zI} \quad (C7f)$$

$$\bar{C}_{m\alpha R} = C_{m\alpha R} - h(C_{mzR} - C_{\ell\alpha R}) - h^2C_{\ell zR} \quad (C7g)$$

$$\bar{C}_{m\alpha I} = C_{m\alpha I} - h(C_{mzI} - C_{\ell\alpha I}) - h^2C_{\ell zI} \quad (C7h)$$

The equations in (C7) are a linear combination of the original derivatives referred to the mid-chord. These equations apply when the reference axis is moved aft of the mid-chord a distance  $h\ell$  towards the trailing edge.

## VITA

Louis Kronenberger, Jr. was born on January 10, 1944 in Ft. Worth, Texas. His parents relocated to Houston, Texas in 1950 and he consequently received his primary and secondary education in the Houston Independent School District.

After graduating from high school in 1962, he attended Texas A&M University where he received a Bachelor of Science degree in 1966, majoring in aerospace engineering and receiving a commission as a Second Lieutenant in the U.S. Army. Prior to reporting for active duty, he worked for LTV Aerospace Corporation in Dallas, Texas in their Structures Group.

In May, 1967 he entered on active duty with the Army. He is presently still on active duty and holds the rank of Major. His military experience includes in excess of 2000 hours of flight experience in various fixed and rotary wing aircraft. His career specialties are in Aviation and Research and Development and he has received related assignments in these two specialties.

In September, 1976 the Army presented him with the opportunity to return to Texas A&M University to do graduate work in aerospace engineering. Upon completion of the requirements for a Master of Science degree, Major Kronenberger will be assigned to the CH-47 Project Manager's Office, Aviation Systems Command, St. Louis, Missouri.

His permanent mailing address is P.O. Box 875, Arlington, Texas 76010.

78